Seminar series nr 131

Spatial Distribution of Hydraulic Conductivity in the Rio Sucio Drainage Basin, Nicaragua

A Minor Field Study

Magnus Eckeskog

2006
Geobiosphere Science Centre
Physical Geography and Ecosystems Analysis
Lund University
Sölvegatan 12
S-223 62 Lund
Sweden

Spatial Distribution of Hydraulic Conductivity in the Rio Sucio Drainage Basin, Nicaragua

A Minor Field Study

Magnus Eckeskog, 2006

Master's Degree thesis in Physical Geography and Ecosystem Analysis

Supervisors

Andreas Persson and Alfredo Mendoza

Department of Physical Geography and Ecosystems Analysis

Lund University

Acknowledgements

Great thanks to my supervisors:
Dr. **Alfredo Mendoza** for inviting me to take part in his PhD project in Nicaragua, and for introducing me to the Nica ï culture;
Dr. **Andreas Persson** for believing in my project, helping me to carry out over all planning and GIS analysis in Sweden and;

Also great thanks to Dr. **Harry Lankreijer** for strategic support, encouragement to start searching for an MFS project, and for always keeping the door open for project discussions.

I would further like to thank:
Julio César Guevara Pérer for fieldwork assistance and path-finding in the sometimes very challenging terrains. The family Monje: **Don Ramiro** for field assistance. **Doña Lastenia** for nice conversations, great gallo pinto, and good advice. **Lesbia**, **Heidi**, and **Chester** for friendship entertainment, and a helping hand during fieldwork. The staff at CIGEO, for the nice company in Managua, and for providing with the laboratory facilities. **Roger Blandón** for excellent driving skills and nice company in Santo Domingo. Family and staff at El Comedor Esquina Dorada for great company and good food.

Emilie Stroh at the GIS Centre, Lund University, for putting me into contact with Alfredo Mendoza. Dr. **Jonas Åkerman** at the department for Physical Geography and Ecosystem analysis, Lund University (INES), for inspiring me to choose the interesting, but not always marked out path. **Karin Larsson** at the GIS Centre, Lund University, for providing me with GIS software. **Pablo Morales** at INES, for Spanish proofreading.

Students, teachers and staff at INES, for classes, knowledge, and memorable times.

Family and friends, for support and encouragement.

I also wish to give gratitude to the Swedish International Development Cooperation Agency (SIDA) and the Earth Sciences Centre in Gothenburg for making this project possible by providing funding through the Minor Field Study (MFS) Programme.

Finally, thank you **Nina**, without you I would have been completely lost, not only in the vast Nicaraguan bush, but also in life in general. Your support and patience has been, and continues to be, invaluable.

Abstract

The central mountainous region of Nicaragua is an area subjected to heavy environmental pressure due to anthropogenic activities. For over a hundred years mercury has been used in gold mining activities in this area causing pollution of water resources. The lack of infrastructure in this region has made investigations regarding water quality and availability scarce. This work is focused around the drainage basin of the river Rio Sucio which belongs to the catchment area of the river Rio Escondido, one of the most polluted watersheds in Nicaragua. The work is a Minor Field Study (MFS), and is part of a project which aims at strengthening the scientific capabilities of Nicaraguan universities to solve problems related to groundwater resource management. Previous studies within the project have found high concentrations of Mercury (Hg) and Lead (Pb) in water, sediments, and soils of the Rio Sucio river basin. This has called for an increased knowledge regarding the groundwater systems of the area. Recent and ongoing studies in the area have concluded that there is a need to understand the ground water and the surface water interactions of the area in order to assess the contamination risk of the ground water. One of the missing links in understanding these interactions is the infiltration characteristics of the soils of the area. This project was therefore commissioned by Centro de Investigaciones Geoscientificas (CIGEO) in order to investigate the saturated hydraulic conductivity (K_{sat}) in the unsaturated zone of the Rio Sucio river basin. The primary objective of this work is to carry out measurements of K_{sat} in the unsaturated zone, and to investigate whether or not values of K_{sat} show any patterns of autocorrelation. This work also investigates if K_{sat} in the study area is dependent on geological features and geomorphological characteristics. A hundred sampling points were distributed over a 25 Km^2 large area. At each location K_{sat} was determined with a Constant Compact Head Permeameter (CCHP). Recordings of degree of slope and soil samples were collected at each location. The recordings of K_{sat} were compared with digital maps of geology, a Digital Elevation Model, soil particle size, and slope. Geostatistical analysis was performed on the K_{sat} samples. Values of K_{sat} ranged from 0.0028 cm/h to 10.43 cm/h, giving a five order difference in magnitude. The study area was dominated by low values of K_{sat}; 58% of the samples showed a K_{sat} lower than 0.34 cm/h, and 68% showed a K_{sat} lower than 1 cm/h. Only 17% of the samples showed a K_{sat} above 2.67 cm/h. There was no autocorrelation found in the data, and there was no correlation found between K_{sat} and the investigated factors. More detailed studies of the infiltration characteristics of the area at a finer resolution are recommended for future hydrological studies of the area.

Keywords: Geography, Physical Geography, GIS, Saturated hydraulic conductivity, Geostatistics, Interpolation, Constant Compact Head Permeameter, Hydrogeology, Hydrology, Geomorphology, Geology, Soil.

Sammanfattning

Vattendragen i Nicaraguas centrala bergsområden är utsatta för hög miljöpåverkan. I över hundra år har kvicksilver använts för att utvinna guld i dessa områden, vilket förorenat vattenresurserna. Det har gjorts få undersökningar av områdets vattenkvalité, vilket främst beror på avsaknaden av infrastruktur. Detta arbete är koncentrerat kring floden Rio Sucio, vilket tillhör Rio Escondidos avrinningsområde, ett av de mest förorenade vattendragen i Centralamerika. Arbetet är ett Minor Field Study (MFS), och är en del av ett större projekt vilket syftar till att öka den vetenskapliga kompetensen hos Nicaraguas universitet att lösa grundvattenresursrelaterade problem. Tidigare delprojekt har påvisat höga halter av kvicksilver (Hg) och bly (Pb) i vatten, sediment och jord i Rio Sucios avrinningsområde. Därmed finns en potentiell risk att grundvattnet och därmed dricksvattnet blir förorenat av tungmetaller. Detta ledde till ett behov av att utreda områdets hydrogeologiska egenskaper, samt samband och interaktioner mellan områdets yt- och grundvatten. För att kunna göra detta behövs kunskap om infiltrationsegenskaperna hos områdets jordlager. Detta projekt gjordes på uppdrag av Centro de Investigaciones Geoscientificas (CIGEO), med syftet att undersöka mättad hydraulisk konduktivitet (K_{sat}) i områdets omättade jordlager, samt att utreda huruvida uppmätta värden av K_{sat} påvisade några mönster av autokorrelation. Studien undersöker vidare om K_{sat} i området är beroende av geologiska och geomorfologiska egenskaper. Hundra mätpunkter distribuerades över ett 25 km^2 stort område. Vid varje mätpunkt bestämdes K_{sat} med hjälp av en Compact Constant Head Permeameter. Mätningarna av K_{sat} jämfördes med geologikartor, en Digital Elevation Model, kornstorlek, samt sluttning. Insamlad K_{sat} undersöktes också geostatistiskt efter autokorrelation. K_{sat} varierade i storlek från 0,0028 cm/h till 10.43 cm/h över området. Området dominerades av låga värden; 58% av proverna påvisade en K_{sat} lägre än 0,34 cm/h och 69% lägre än 1 cm/h. Endast 17% av mätningarna visade en K_{sat} högre 2,67 cm/h. Ingen autokorrelation hittades i insamlad data, och det gick ej heller att påvisa någon korrelation mellan K_{sat} och de övriga undersökta faktorerna. För att få fram kvalitativa resultat rekommenderas att studier över områdets infiltrationsegenskaper görs med en betydligt finare upplösning, samt med fokus på färre antal faktorer.

Nyckelord: Geografi, Naturgeografi, GIS, Mättad hydraulisk konduktivitet, Geostatistik, Interpolering, Constant Compact Head Permeameter, Hydrogeologi, Hydrologi, Geomorfologi, Geologi.

Resumen

La parte centro-este de Nicaragua, es un área sujeta a impacto ambientales causados por actividades antropogénicas. Por más de cien años el mercurio (Hg) ha sido usado en las actividades mineras en el centro de Nicaragua, causando contaminación de recursos aguas. La ausencia de infraestructura en esta área ha hecho que las investigaciones sobre la calidad y acceso de agua sean muy escasas. Este proyecto se focaliza en los alrededores de la cuenca del Rio Sucio que pertenece a la cuenca de Río Escondido, uno de los ríos mas contaminados de Centro América. El proyecto es un Minor Field Study (MFS), y es parte de un proyecto que intenta mejorar las capacidades de las Universidades Nicaragüenses para resolver problemas relacionados con la administración de recursos hídricos. En estudios previos se ha encontrado alto contenido de mercurio (Hg) y plomo (Pb) en muestras de agua, sedimento y suelos en la cuenca del Río Sucio. Esto exige más conocimiento de las relaciones e interacciones del agua subterránea y el agua superficial para evaluar el riesgo de que el agua subterránea sea contaminada. Uno de los partes que faltan para entender estas relaciones es el conocimiento de las propiedades de la infiltración hidráulica de los suelos del área. En éste sentido, este trabajo fue encargado con el objeto de investigar la conductividad hidráulica (K_{sat}) en la zona no saturada de la cuenca de Río Sucio. El primer objetivo de este estudio es hacer mediciones de K_{sat} en la zona no saturada e investigar si K_{sat} tiene autocorrelación. Además, este trabajo intenta investigar si hay relaciones entre características geológicas y geomorfología.

En cuanto a la metodología, cien puntos fueron distribuidos sobre un área de 25 km^2. En cada lugar K_{sat} fue determinado con un Constant Compact Head Permeameter (CCHP). Mediciones de lixiviación de la topografía y muestras de suelo fueron colectadas en cada lugar también. Las mediciones de K_{sat} fueron comparadas con mapas digitales de geología y un Digital Elevation Model (DEM), para tamaño de la partícula de suelo y lixiviación de la topografía. Además K_{sat} fue investigado para autocorrelación, con un semivariogram. Los valores de K_{sat} variaron de 0.0028 cm/h a 10.43 cm/h lo cual significa una diferencia de cinco magnitudes. En el área de estudio predominaron valores bajos de K_{sat}; 58% de las mediciones mostraron menos que 0.34 cm/h y 68% menos que 1 cm/h. Solo 17% de las mediciones mostraron un K_{sat} superior a 2.67 cm/h. No hubo autocorrelación en los datos colectados y tampoco hubo ninguna correlación entre K_{sat} y los además factores investigados. En el futuro, se recomiendan estudios mas detallados de las características de la infiltración del área en una resolución mas fina.

Table of contents

1 Introduction

Following the global increase in fresh water demand, together with water pollution caused by anthropogenic activities, there is a call for investigations and research of groundwater resources. In Nicaragua, as in many other developing countries, there is a lack of knowledge regarding the availability of groundwater aquifers and the interactions between surface and groundwater. This is particularly evident in the central mountainous regions, due to the lack of infrastructure.

Human activities like farming and gold mining put heavy stress on the watersheds, causing severe pollution. The river Rio Sucio belongs to the catchment area of Rio Escondido, which is one of the most environmentally endangered watersheds in Nicaragua. In the Rio Sucio river basin substantial amounts of mercury (Hg) has been found. The mercury originates from gold mining activities where it is used in the gold refining process. The Mercury concentrations in the surface water have shown to be higher than WHO recommended drinking standards (Mendoza, 2002). Moreover, high contents of lead (Pb) have been found in the river water, exceeding US EPA drinking water standards (Grunander and Nordenberg, 2004). The lead presumably originates from the ore, and occurs naturally in the minerals of the area. Hence, this pollution source may be attributed to the mining activities as well. Further stress is put on the river due to the very poor sanitary facilities in these areas. The river is used as latrine system, as well as dump site of house hold garbage (Grunander and Nordenberg, 2004).

It is of great importance to investigate the groundwater resources in these areas, in order to clarify whether they respond to future demands for human consumption or not. Moreover, to determine the risk for the groundwater of becoming polluted, it is necessary to examine the interactions between surface water and groundwater.

This thesis is part of a project called ñAquifer vulnerability due to local contamination in the Rio Mico and Rio Sucio river basinsò, carried out by Centro de Investigaciones Geoscientificas (CIGEO) and the University of Lund, established in 1998. The project is within the framework of a major multidisciplinary environmental research programme, funded by the Swedish International Development Cooperation Agency (SIDA) and The Department for Research Cooperation (SAREK). The programme aims to strengthen the

scientific capabilities of Nicaraguan universities to solve scientific problems related to ground water resource management.

This project is a continuation of previous work carried out in the Rio Sucio river basin by Alfredo Mendoza at CIGEO which aims at establishing a base of information about the hydrogeological conditions in the area. One of the main objectives in his project is to evaluate the hydraulic relations between surface water, upper groundwater aquifers and deeper seated aquifers. The idea is to gradually create a hydrogeological map. In order to achieve this, Mendoza (2002) concluded that the hydraulic conductivity (permeability) of the soils in the Rio Sucio river basin needs to be investigated.

Therefore this project was commissioned by CIGEO who wish to evaluate the spatial distribution of the saturated hydraulic conductivity (K_{sat}) in the unsaturated zone of the Rio Sucio river basin. It is of great interest to discern if it is possible to interpolate values of K_{sat}, which would be a step closer towards producing a hydrogeological map. A method proposed by CIGEO was therefore used in order to carry out the investigation. All the materials needed to carry out the investigation method were provided by CIGEO in Nicaragua.

1.1 Objectives

The primary objectives of this study are:

-to carry out measurements of saturated hydraulic conductivity (K_{sat}) in the unsaturated zone of the Rio Sucio river basin, and thereby investigating the general infiltration characteristics of the soils in the study area.

-to study the spatial distribution of K_{sat}, i.e. to see whether values of K_{sat} in sampling points close to each other are more similar than sampling points at longer distances.
This will show whether or not it is possible to interpolate these values and produce a map of K_{sat}.

Moreover, this project seeks to study the relationship between K_{sat} and prevailing conditions of geology and geomorphology of the study area in order to try to explain the spatial distribution of $K_{sat.}$ More specifically this was done by:

-investigating whether K_{sat} in the unsaturated zone is dependent on particle size, type of underlying bedrock, quartz veins, and fractures/faults in the bedrock.

-studying whether the distribution of K_{sat} is dependent on slope and elevation.

1.2 Geography of Nicaragua

Nicaragua is located in Central America bound by Honduras to the north, Costa Rica to the south the Caribbean Sea to the east and the Pacific ocean the west. The country covers a total area of 129,494 square kilometres (120,254 square kilometres of which are land area) making it the largest country of Central America. It contains a diversity of climates and terrains (Merrill, 1994). Nicaragua is one of the Western Hemisphere's poorest countries. It has a low per capita income, widespread underemployment, and a heavy external debt burden. The country has 5 570 129 (CIA, 2006) inhabitants which are divided into four different ethnical groups; Mestizo, White, Indian, Black and Mulatto (Merrill, 1994).

1.2.1 Physical Geography

The physical geography of Nicaragua can be divided into three major zones: Pacific lowlands, the more humid, cooler central highlands, and the Caribbean lowlands.

The Pacific lowlands reach about 75 kilometres inland from the Pacific coast. Most of the area is flat, apart from a row of young volcanoes, between the Golfo de Fonseca and Lake Nicaragua. Many of the Volcanoes are still active. The Volcanoes form peaks that are an extension of The Costa Rica Highlands, which fade out to the South into the low Rivas Isthmus. West to the peaks a large crustal fracture or structural rift is situated, which forms a long, narrow depression running southeast across the isthmus from the Golfo de Fonseca to the river Río San Juan (Merrill, 1994) (fig 1).

In the rift lie the largest freshwater lakes in Central America: Lago de Managua (56 kilometres long and 24 kilometres wide) and Lago de Nicaragua (about 160 kilometers long and 75 kilometers wide). These two lakes are attached by the river Río Tipitapa, which flows south into Lago de Nicaragua. Lago de Nicaragua consecutively drains into the river Río San Juan (the boarder between Nicaragua and Costa Rica), which flows all the way through the

southern part of the rift lowlands to the Caribbean Sea. The valley of the river Río San Juan forms a natural passageway close to sea level across the Nicaraguan isthmus from the Caribbean Sea to Lago de Nicaragua and the rift (Merrill, 1994) (fig 1).

Figure 1: Map of Nicaragua, shaded relief. From: Perry-Castañeda, (1997).

Adjacent to the lakes and extending northwest of them along the rift valley to the Golfo de Fonseca, there are fertile lowland plains greatly enriched with volcanic ash from nearby volcanoes. West of the lake region lies a thin line of ash-covered hills and volcanoes that divide the lakes from the Pacific Ocean. This line is highest in the central part near León and Managua (Merrill, 1994) (fig 1).

Western Nicaragua is situated where two major tectonic plates collide, and is consequently subjected to earthquakes and volcanic eruptions. Although intermittent volcanic eruptions have caused agricultural damage from fumes and ash, earthquakes have been considerably more destructive to life and property. Hundreds of shocks arise each year, some of which cause severe damage. Major parts of the capital city of Managua were destroyed in 1931 and again in 1972 (Merrill, 1994).

A triangular area referred to as the central highlands is situated northeast and east of the Pacific lowlands. This rugged mountain terrain consist of ridges 900 to 1,800 meters high and a mixed forest of oak and pine alternating with deep valleys that drain primarily towards the Caribbean. The Central Highlands form part of the volcanic ranges that begin in the Alaskan Mountains and continue through to the Rocky Mountains, the islands of the West Indies and the Andes to Cape Horn (Merrill, 1994) (fig 1).

Not many significant streams flow west to the Pacific Ocean; those that do are steep, short, and flow only irregularly. The central highlands are divided into two parts; -the relatively dry western slopes protected by the ridges of the highlands from the moist winds of the Caribbean, -and the eastern slopes of the highlands covered with rain forests (Merrill, 1994).

The eastern Caribbean lowlands of Nicaragua form the wide-ranging (constituting more than 50 percent of national territory) and sparsely populated lowland area known as Costa de Mosquitos. The Caribbean lowlands are hot and humid areas including coastal plains, the eastern side tracks of the central highlands, and the lower segment of the Río San Juan drainage basin. The soil is generally leached and infertile. These areas are predominated by pine and palm savannah. Tropical rain forests are characteristic from the Laguna de Perlas to the river Río San Juan, in the interior west of the savannas, and along rivers through the savannas. Fertile soils are constrained to the natural levees and narrow floodplains of the numerous rivers, including the Escondido, the Río Grande de Matagalpa, the Prinzapolka, and the Coco, as well as along the many lesser streams that rise in the central highlands and cross the region on the way to the composite of shallow bays, lagoons, and salt marshes of the Caribbean coast (Merrill, 1994).

1.2.2 Climate

There is little variation of temperature with seasons in Nicaragua; it is more a function of elevation. The *tierra caliente* (hot land), is characteristic of the foothills and lowlands from sea level to about 750 meters of elevation. In these areas, daytime temperatures average 30° C to 33° C, and night temperatures drop to 21° C to 24° C most of the year. The *tierra templada* (temperate land), is characteristic of the majority of the central highlands, where elevations range between 750 and 1,600 meters. These areas have mild daytime temperatures between 24° C to 27° C, and the nights are cool with temperatures around 15° C to 21° C. *Tierra fría* (cold land), at elevations above 1,600 meters, is found only on and adjacent to the highest peaks of the central highlands. Daytime averages in this region are 22° C to 24° C, with night time lows below 15° C (Merrill, 1994, Schwerdtfeger, 1976).

There is a great variation in rainfall in Nicaragua. The wettest region of Central America is found in the Caribbean lowlands, receiving between 2,500 and 6,500 mm of rain annually. The western slopes of the central highlands and the Pacific lowlands receive significantly less annual rainfall, since they are protected from the moisture laden Caribbean trade winds by the peaks of the central highlands. Mean annual precipitation for the rift valley and western slopes of the highlands ranges from 1,000 to 1,500 mm. Rainfall is seasonal, May through October is the rainy season, and the driest period is found from December to April (Merrill, 1994, Schwerdtfeger, 1976).

Heavy flooding occurs along the upper and middle reaches of all major rivers during the rainy season. Close to the coast, where river courses widen and river banks and natural levees are low, floodwaters spill over onto the floodplains until large sections of the lowlands become continuous sheets of water. The coast is also subjected to destructive tropical storms and hurricanes, particularly from July through to October. Considerable destruction of property is often caused by the high winds and floods accompanying these storms. Heavy rains associated with the passage of a cold front or a low-pressure area may sweep from the north through both eastern and western Nicaragua, particularly the rift valley, from November to March. Hurricanes or heavy rains in the central highlands, where agriculture and mining has replaced much of the natural vegetation, also cause considerable crop damage and soil erosion (Merrill 1994, Schwerdtfeger, 1976). E.g., Hurricane Joan in 1988, and Hurricane Mitch in

1998 caused severe damages in Nicaragua. Both claimed many lives, and forced hundreds of thousands Nicaraguans to flee their homes (NOAA, 2004).

1.2.3 Geology

Nicaragua is located on the western margin of the continental Caribbean plate. The Central American region can be divided into two large units, which differ completely from each other in terms of geology and structures. The northern part is called the Chortis block and contains Guatemala, Honduras, El Salvador, and the northern parts of Nicaragua (fig 2). This part is composed of a continental type crust with Palaeozoic to pre-Tertiary rocks. The southern part is an uplifted oceanic slice of early Jurassic age, called the Chorotega block, which contains The southern parts of Nicaragua, Costa Rica, and Panama (fig 2) (Rodriguez, 1994). The greater part of Nicaragua is located on the Chortis block, and this is also where the study area is located. The Chorotega block will therefore not be further explained.

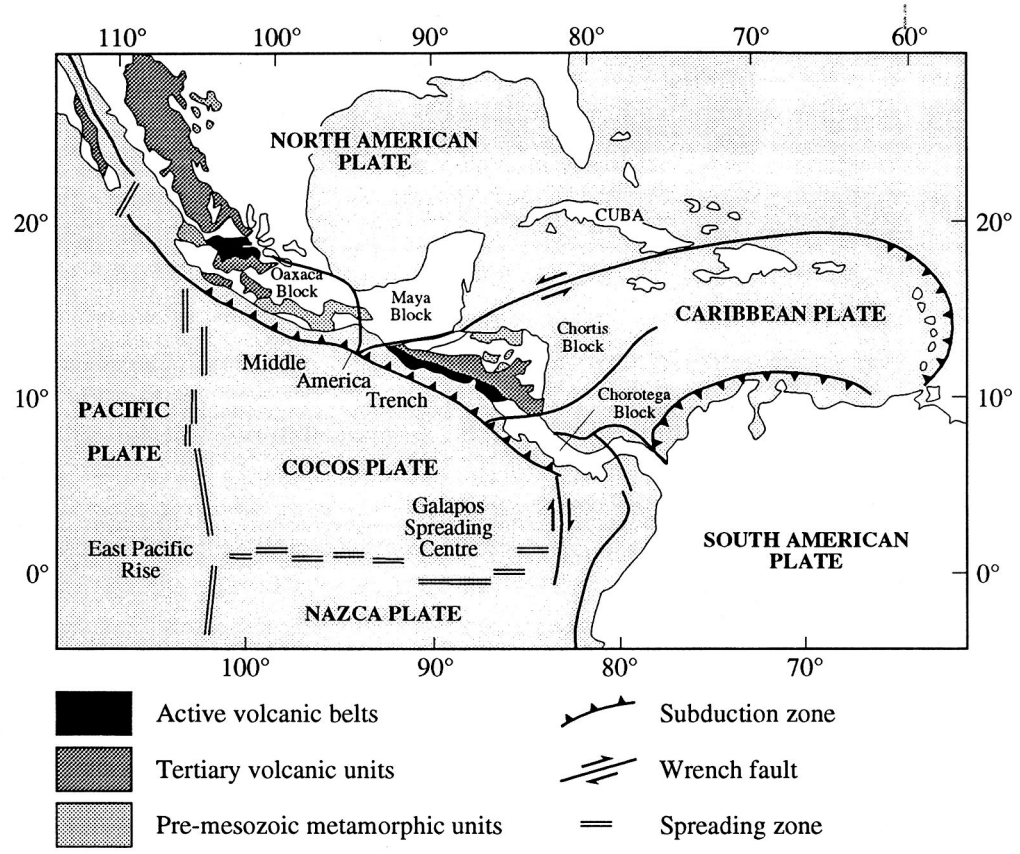

Figure 2: Geology of Central America. From Leytón, 1994.

Four different kinds of geological terrenes are distinguished within the Chortis block: the Pacific Coastal plain, the Nicaraguan Depression, the interior Highlands, and the Atlantic Coastal Plain (Leytón, 1994).

The Pacific Coastal plain forms a narrow strip between the south-western margin of the depression and the Pacific Ocean from the Coseguina peninsula across the plains of Chinandega and Leon, and along the Sierras de Carazo to the narrow isthmus of Rivas. The Pacific Coastal Plain has units of sedimentary and volcanic origin, ranging in age from late Cretaceous to Pliocene. It is bounded on the northeast by the chain of active volcanoes and the fault system along the pacific side of the Nicaraguan Depression (Leytón, 1994).

Within the Nicaraguan Depression a thick accumulation of alluvium, lake sediments, and deeply weathered volcanic ash cover all but a few isolated hills of Tertiary rocks. A quaternary volcanic front follows the western inner side of the depression (fig 3) (Leytón, 1994).

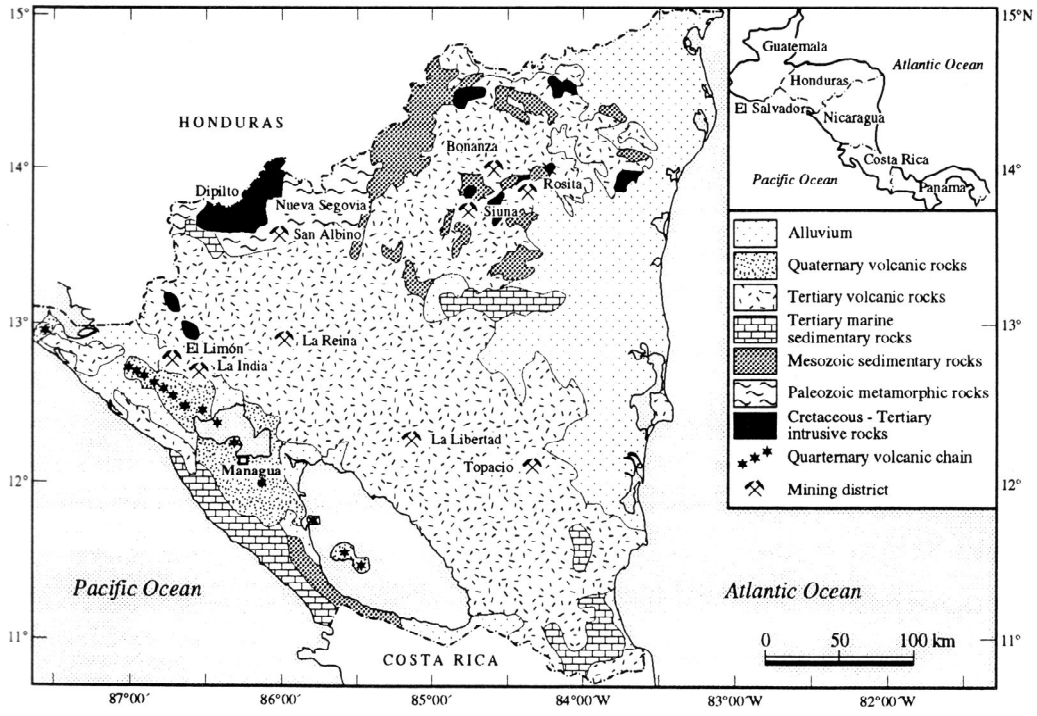

Figure 3: Geology of Nicaragua. From Rodriguez, 1994.

Northeast of the depression, the Interior Highlands rise in a series of gently tilted and deeply dissected volcanic deposits of Tertiary age. The Tertiary volcanic sequence has been divided

into two main units, the older Matagalpa Group, which is characterized by predominantly intermediate to felsic rock associations and the Coyol Group characterized by mafic lavas and dacitic to andesitic igimbrites. Small exposure of sedimentary rocks is present within the Tertiary volcanic series along the eastern slopes of the Interior Highlands (Mc Birney and Williams, 1965).

A topographic backbone of Nicaragua is created by a mountain ridge which gives way to the rain forests of the Atlantic Coastal Plain. This mountain ridge mainly consists of Miocene to Quaternary sedimentary and volcanic formations, which over most of the area cover the Paleozoic-Meozoic basement (fig 3) (Leytón, 1994).

1.3 Study area

The study area is located in Chontales, central region of Nicaragua. Santo Domingo, a small village is situated in the northern part of study area, at a distance of approximately 177 km from Managua, the capital of Nicaragua (fig 4). The infrastructure in this part of Nicaragua is very poor. Santo Domingo can be reached by a 5h drive from Managua. The field investigation area is characterised by a hilly landscape with scarce and small plains, creating a fairly high relief. The area is cut through from north to south by a river, called Rio Sucio, which means ñdirty riverò. Rio Sucio is a tributary to the river Rio Siquia, which meanders towards the Caribbean Sea.

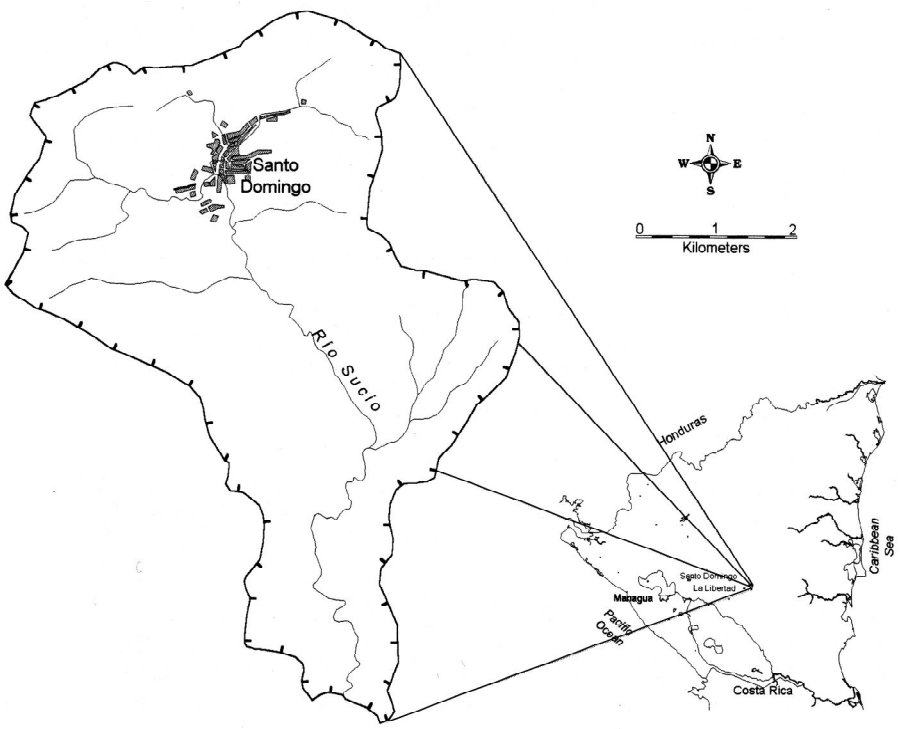

Figure 4: Study area. The drainage basin of Rio Sucio in central Nicaragua. The village of Santo Domingo is located in the northern part of the study area. Mod after Mendoza 2002.

1.3.1 Geography and climate of Santo Domingo

The drainage area of Santo Domingo has an average annual temperature between 23 and 24 degrees, with an average rainfall of 2424 mm. The area is characterized by a mixture of tropical savannah and tropical monsoon forest with two seasons: rain season from April to December, and dry season from December to March. The vegetation types present are strongly dependent on the water availability, and the disturbance put on by mining, grazing and deforestation. Cattle grazing and deforestation have caused extensive areas of open fields, often subjected to erosion (fig 5).

Fig 5: Area subjected to erosion as a result of deforestation followed by cattle grazing and mining.

Savannah consisting of shrub, grass, and scarce tree -vegetation is represented on plains and plateaus (fig 6), and monsoon forest with more green and lush dense tree -vegetation in the valleys where the river meanders (fig 6). The prevailing wind direction in the area is from the Northeast, at an average speed of 3.8 m/s.

Fig 6: Plains and plateaus consisting of Savannah, and valleys dominated by monsoon forest.

1.3.2 Geology

The geology of the study area is dominated by Cenozoic Tertiary igneous rocks. The area is divided into two main stratigraphic units, the Coyol Group (Miocene-Pliocene age) and the older Matagalpa Group (Oligocene-Miocene age). The Matagalpa group is characterized by intermediate to acid pyroclastic rocks, and the Coyol group by basic lavas and dacitic to

andesitic ignimbrites (Darce, 1989). These tertiary igneous and volcaniclastic rocks are part of a northwest-southeast belt through Central Nicaragua. The belt consists of basic lava, acid and intermediate pyroclastic volcaniclastic sedimentary rocks (Weinberg, 1992).

In the beginning of tertiary time, tension forces affected the mountain chain, which made up welling magma and acid rest solutions leak into fractures. This in turn created quartz veins containing layers of feldspar and other minerals (fig 7). As these minerals are weathered, clay minerals are released from the quartz veins. This can result in two things. The clay minerals may close the veins so they act as a barrier to water flow, or the flow opens up the veins more, resulting in a better water conductance. This is depending on whether the clay minerals deposit on the veins or is transported elsewhere.

The quartz veins contain ore, and it is possible to find gold in the weathered material in, and in the close vicinity of the veins (Aronsson and Wallner, 2002).

Fractures, faults, and quartz veins are distributed in a northeast-southwest direction in the study area. Transversal faults are to be found in a northwest-southeast direction, which have led to block movements (Aronsson and Wallner, 2002) (fig 7).

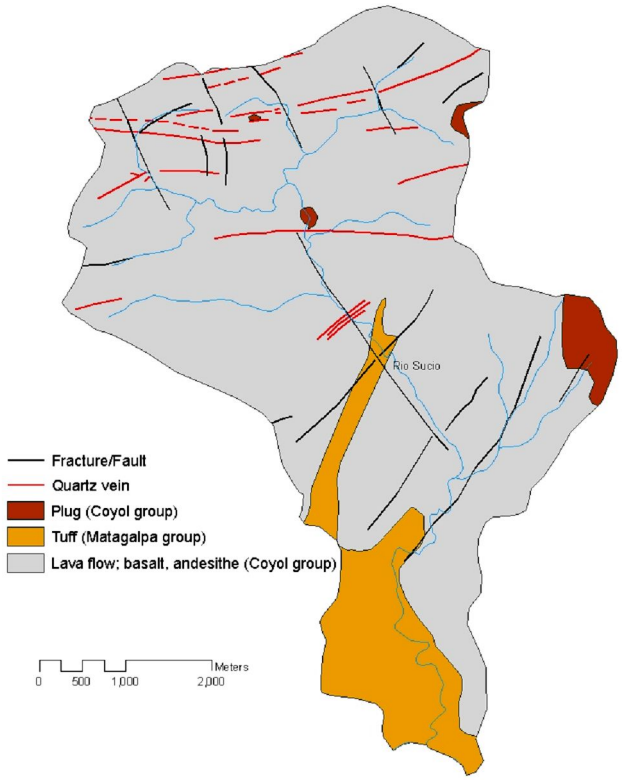

Figure 7: Major geological units of the study area. Mod after Mendoza, 2002.

The main rock types of the study area are the igneous rocks basalt, andesite, rhyolite, and pyroclastic rocks. Three distinct geological units can be recognized in the study area.

The largest geological unit, covering approximately 80% of the area consists of lava flows, basalts, and andesites, which are parts of the Coyol group (fig 7). The second unit covering approximately 10% of the area is made up by tuff, which is a pyroclastic rock with high porosity (fig 7). Tuff originates from small particles of ash and dust ejected during volcanic eruptions, which eventually hardens (Strahler and Strahler, 2000). This geological unit covers the southern part of the area and belongs to the Matagalpa group. The third geological unit is found in the southeast corner of the basin and at some locations in the north. This unit mainly consists of rhyolite and rhyodacite, and has formed volcanic plugs (fig 7). This unit belongs to the Coyol group (Mendoza, 2002).

The soils covering the study area are derived from the previously mentioned rocks. Little investigations about soil types have been made in the area, and no detailed soil map over the study area exists (Mendoza pers comm, 2005). The soils mainly consist of clay with variable contents of silt corresponding to the associations of Orthoxic Tropudults and Typic Tropodults, according to USDA classifications (INETER, 1973). In some areas in the south a more silty clay soil can be found. The soils often have a brown reddish colour, rather fine textured (fig 8 a). Closer towards the quartz veins the soils turn redder in their colour, most likely caused by ferric oxides. These soils have a somewhat coarser texture (fig 8 b).

A **B**

Fig 8: A) The most common appearance of the soils in the study area. **B)** Reddish soil surrounding a quartz vein.

The soils derived from pyroclastic acid rocks have a grey colour and a fine texture (Mendoza pers comm, 2005, Personal observations).

1.3.3 Mining in Santo Domingo

These days the mining industry is not a very important part of the Nicaraguan economy. Not more than 1 tonne gold/year and 3 tonnes silver/year is extracted from Nicaraguan mines. However, in Santo Domingo mining is the principal source of income together with agriculture and cattle-raising. About 400 hundred households (2500 inhabitants) are dependent on mining as their primary source of income (Aronsson and Wallner, 2002).

The mining industry of Santo Domingo started in 1910. The mines are exploited manually with equipment like shovels, hoes, crowbars, hammers, and chisels. Shafts are made into quartz veins in order to extract the gold, after which the ore is brought to a processing plant where it is crushed and grinded. The rocks are pulverised with pestles, and cyanide and water

is added. The mixture is poured over an inclined copper plate covered with mercury for extraction of the gold. When as much gold as possible is extracted, the leftovers are discharged into the river Rio Sucio (Aronsson and Wallner, 2002).

2 Theoretical background

2.1 Water movement in soil

Water movement in soil consists of essentially three types of movements, determined by the readily available water in the soil. The amount of water decides whether the movement is saturated, unsaturated or by vapour transfer (Fitzpatrick, 1986). Saturated flow occurs when all of the pores are filled with water. This usually occurs beneath the water table but also when ever a soil becomes saturated, e.g. on occasions with heavy rains. Saturated flow may be in any direction. The rate of flow is determined by the hydraulic conductivity and the hydraulic gradient (Fitzpatrick, 1986).

Unsaturated flow occurs when there is a considerable amount of air in the large pore spaces, and water moves from pore to pore by flowing over the surfaces of aggregates and/or particles. In soils that have recently been soaked the flow is downwards in response to gravity. However, as field capacity is reached movement is usually either lateral or upward by capillarity in response to a moisture gradient due to drying at the surface or uptake by plant roots. Hence, unsaturated flow takes place in response to gravity as well as in response to a moisture gradient (Fitzpatrick, 1986).

Vapour transfer takes place as water in the vapour phase moves from one place to another in the soil and from the soil to the atmosphere. The relative humidity, the temperature gradient, the size and the continuity of the pores, and the amount of water present, determines the rate of movement (Fitzpatrick, 1986).

Henry Darcy (1856) gave the first quantitative description of water movement through a porous medium (Marshal and Holmes, 1979). Darcyôs law describes most of the water flow that takes place in soils (Campbell and Norman, 1998) (equation 1).

Soil water movement is very complex, due to the intricate structure of the soil matrix. Soil pores are irregularly shaped convoluted and complexly interconnected. Flow through pores is limited through numerous constrictions. Therefore, when describing the water flow in soil, a general water flow pattern is usually derived called a macroscopic flow-velocity vector. This is the overall average of the microscopic velocities over the total volume considered. Hence,

the conducting body is treated as a uniform medium, with the flow spread out over the entire cross section, solid and pore space alike (Hillel, 2004). The macroscopic velocity (v) is defined with the law of Darcy:

$$v = Q/A = -K * d\varnothing / dx \quad (1)$$

Where:

Q = *rate of water discharge (m^3/s)*

A = *cross sectional area of the actual soil layer (m^2)*

K = *hydraulic conductivity (m/s)*

$\varnothing$ = *total water potential (m)*

x = *distance (m)*

$d\varnothing / dx$ = *change in total potential per length unit, potential gradient (m/m)*

Q/A is measured in m/s, and is sometimes referred to as Darcy velocity (v_d).

Darcyôs law is primarily designed for saturated flow, but it has also shown to be true for unsaturated flow (Grip and Rhode, 2003). The law states that the flow between two adjacent points in the ground is proportional to the total difference in potential between the two points. Hence, for unsaturated flow the equation expresses that the flow normally is directed downwards (lower energy potential) and towards drier areas (lower pressure potential) (Grip and Rhode, 2003).

2.1.2 Soil water potential

The total potential of water is the sum of the gravitational, pressure and osmotic -potentials. Wherever the potential differs it experiences a force that tends to move it from positions of greater energy to those of lesser magnitude. The influence of osmotic potential can often be neglected since it is confined to cases where salt sieving occurs, as for example by plant roots. The sum of the gravitational and the pressure -potential is called the hydraulic potential (Marshall and Holmes, 1979).

The soil water potential is commonly referred to as hydraulic head. Hydraulic head means energy per unit weight. This means that hydrostatic pressure can be expressed in the equivalent head of water. A pressure of 1 atm equals a vertical water column, or hydraulic head, of 10.33 m. Since this is a simpler way of expressing soil water potential, the state of

soil water is often referred to as the pressure potential head, the gravitational potential head, and the pressure potential head, normally expressed in meters. The hydraulic head (H) of soil water H, is the sum of the gravitational ($H_{g)}$ and pressure (H_p) ï potential (Hillel, 2004). In other words, H is the sum of the pressure head *h*, and the elevation above a certain datum z (fig 9).

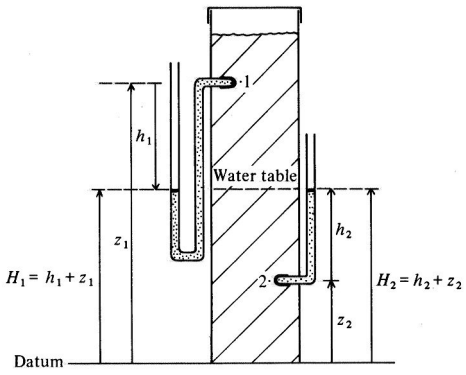

Figure 9: Hydraulic head, H, of water at two points in a soil column, *h* is pressure head and z is the elevation above the datum. From Marshall and Holmes, 1979.

2.1.3 Hydraulic conductivity

Hydraulic conductivity is a function of a porous media and the fluid passing through it. It is commonly used as a measure of the ability for water transport in soils. It is dependent on the distribution and shape of the soil particles, soil particle size, the construction of the soil pores, and the available amount of water in the soil (Fritzpatrick, 1986). The highest rate of hydraulic conductivity for a certain soil is obtained when the entire pore volume is filled with water, i.e. in saturated conditions. The hydraulic conductivity in saturated conditions (K_{sat}) is also referred to as permeability or infiltration rate (Grip and Rhode, 2003).

The hydraulic conductivity is determined by Darcyôs law (equation 1), through measurements of flow and the potential gradient. Determinations of hydraulic conductivity can be made on soil samples in laboratory as well as on entire soil layers in field.

The hydraulic conductivity is strongly dependent on pore size and water availability, which can be illustrated with the velocity of water in a thin tube (equation 2) (fig 10):

$v = \text{constant} * r^2 * d\varnothing / dx$ (2)

Where:

v = mean velocity

r = the radius of the tube

constant = ro*g/(8*my)

ro = the density of the fluid

g = the acceleration of gravity

my = the viscosity of the fluid

Hence, the velocity of the water increases fast with the radius of the tube. This is due to the lacking ability of friction to decrease flow as the radius increases. The discharge (Q) through the tube is given by the velocity (v) times the cross sectional area (A) (equation 3):

$Q = v * A$ (3)

Since both v and A increases with r^2 the discharge (Q) will be increased with r^4 (equation 2 and 3) (Grip and Rhode, 2003). Therefore, the saturated hydraulic conductivity of a soil should increase fast with pore size, and thus with particle size. Coarse textured soils like gravel and sand normally contain a K_{sat} ranging from 10^{-1} to 10^{-5} m/s. In silts K_{sat} can measure between 10^{-4} to 10^{-9} m/s. Clays normally contain a very low K_{sat},, less than 10^{-9} m/s. Note that these are rough estimates of K_{sat} of different soil textures, which are only true for the conductivity that is caused by the pore size distribution of a soil. (Grip and Rhode, 2003).

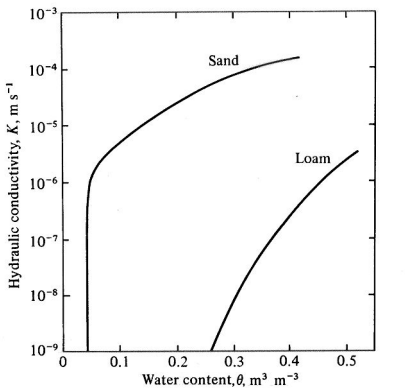

Figure 10: Hydraulic conductivity for a sand and for a loam soil. The effect of particle size and water content is shown. From Marshall and Holmes, 1979.

However, pore size is not the only parameter affecting hydraulic conductivity; the soil structure is another factor strongly affecting conductivity. Hence, water filled fractures and cracks as well as openings created by microbial activity, known as macropores, enhance hydraulic conductivity (Grip and Rhode, 2003).

A condition that a pore will conduct water is that it contains water. This in turn presumes that the pressure of the water does not fall below the binding potential induced by the pore. As a soil begins to dry the conductivity rapidly starts to decrease. This is primarily due to two facts. Firstly because the water content of the cross sectional area is decreasing. Secondly because the larger pores are emptied first (Grip and Rhode, 2003).

Hydraulic conductivity is also strongly affected by erosion and weathering. Rain drop impact can cause disaggregation of soil particles, which may contribute to seal formation processes, and thus decrease hydraulic conductivity (Ramos *et al*, 2003, Ndiaye *et al*, 2005). Human activities may severely affect infiltration capacities of soils. Clearing of vegetation for e.g. agriculture, or mining activities alters the soil characteristics, often making soils highly subjected to erosion by overland flow, altering the hydraulic conductivity of soils. Soil erosion often leads to the reduction of top soil, subsequently decreasing infiltration rates and hydraulic conductivity. This is due to the fact that clay content normally increases with depth (fig 11). Thus, erosion often leads to decreased hydraulic conductivity through exposure of subsoil layers (Veseth 1986). Mining activities often create openings in the bedrock and macropores, which may lead to increased hydraulic conductivity (Guebert and Gardner, 2001).

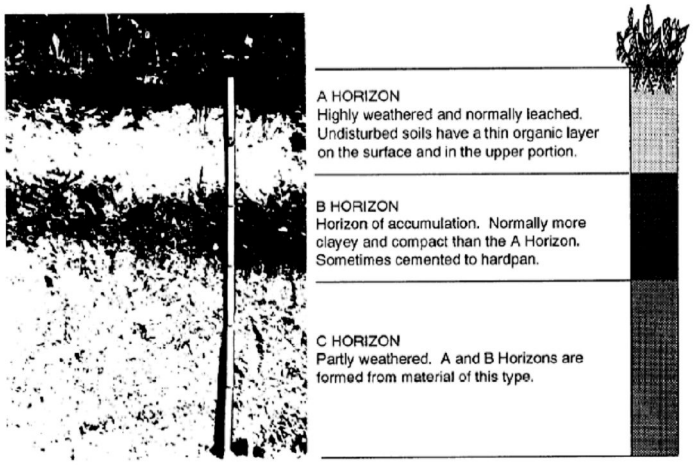

Fig 11: General appearance of a weathering profile developed upon crystalline bedrock. From FM5-410, 1993.

2.2 Interpolation and Digital Elevation Models

Topographic data is normally available as contours or isolines in hard copy maps. When topographic data is desired to be used together with digital raster data, it needs to be presented in raster coverages rather than the original lines. A process of interpolation between the contours enables production of a raster surface which usually is a model of the natural landscape known as a Digital Elevation Model (DEM).

There are two groups of interpolation methods, dividing interpolation techniques into global and local methods. Global methods strive at producing a general trend of the data used, rather than describing the local variation around the different points used. Global methods therefore use all of the points in the dataset as it calculates the unknown cell values. Local interpolation methods on the contrary, use a limited number of values near the cell which is interpolated. In this way local variation is enabled. Trend surface analysis and Fourier transformation constitute examples of global interpolation methods. Thiessen polygons, mean value, and kriging are examples of local interpolation methods. However, there are techniques combining global and local methods, known as spline interpolations. They are computationally efficient interpolation methods, creating smooth surfaces while still maintaining the local variation (Eklundh, 1999).

2.2.1 Interpolation methods

Spline interpolation:

When creating continuous curves between points in a data set, spline functions can be used (equation 4).

$$p(x) = b_0 + b_1 x + \text{é} \quad + b_k x^k, \tag{4}$$

where p(x) is a polynomial, b_0, b_1 xé , b_k the coefficients to be determined, and k the order of the polynomial (Eklundh, 1999). A high order of the polynomial, enables a large local variation of the curve.

When calculations in three dimensions are needed, as in the case with DEMs, bicubic splines can be used (Burrough and McDonell, 1993). By finding the surface with minimum curvature

that passes right through the measured values, a spline function avoids unjustifiable fluctuations. In bicubic splines, polynoms are fitted to a limited number of points. One function joins other functions in the intersections. Since the first and the second derivatives are continuous, a smooth surface is created (Eklundh, 1999).

The thin plate spline introduces a locally smoothed average instead of the strict spline surface. An even surface is generated, at the same time maintaining low residual values between true points and the thin plate functions (Burrough and McDonnell, 1998). This may be convenient when processing topographic data, since objects of natural variation and measurement errors may produce extremely high or low values. This produces a surface with local variation in the terrain, together with smoothness without abnormalities (Eklundh, 1999).

Thin plate spline:

The thin plate spline belongs to the interpolation group of Radial Basis Functions (RBF) (equation 5). RBF:s are theoretically comparable to fitting a rubber membrane through the measured sample values, while at the same time minimizing the total curvature of the surface (Johnston *et al*, 2001). An RBF also known as spline is a local deterministic interpolation technique. It is an exact technique which requires the surface to go through each measured value. The thin plate spline function is explained by the following formula (Johnston *et al*, 2001):

$$Ø(r) = (ů * r)^2 \ln(ů * r) \qquad (5)$$

Where:

Ø(r) is the radial basis function and,

r is the euclidian distance between the predicted location and each data location.

Global polynomial:

The global polynomial interpolation method fits a plane between the sample points based on the general trend of the input data. A plane is a certain case of a family of mathematical formulas known as polynomials. The goal for the interpolation is to minimize error. The interpolation error can be measured by subtracting each measured point from its predicted value on the plane, square it, and add them up. This sum is referred to as a ñleast squaresò fit. This process is the theoretical basis for the first order global polynomial interpolation (Johnston *et al*, 2001).

The Global Polynomial surface changes gradually and captures coarse-scale pattern in the data. The higher the order of the polynomial function, the more variation allowed within the interpolated surface. A first order global polynomial will fit a single plane through the data (equation 6), a second order global polynomial fits a surface with a curve in it (equation 7), a third-order global polynomial allows for two bends (equation 8), and so on (Johnston *et al*, 2001).

First order polynomial (Johnston *et al*, 2001):

$$Z(x_i, y_i) = \beta_0 + \beta_1 x_i + \beta_2 y_i + \varepsilon(x_i, y_i) \quad (6)$$

Where:

$Z(x_i, y_i)$ is the datum at location (x_i, y_i), β_j are parameters, and $\varepsilon(x_i, y_i)$ is a random error.

Second order polynomial (Johnston *et al*, 2001):

$$Z(x_i, y_i) = \beta_0 + \beta_1 x_i + \beta_2 y_i + \beta_3 y^2_i + \beta_4 y^2_i + \beta_5 y^2_i + \varepsilon(x_i, y_i) \quad (7)$$

Third order polynomial:

$$Z(x_i, y_i) = \beta_0 + \beta_1 x_i + \beta_2 y_i + \beta_3 y^2_i + \beta_4 y^2_i + \beta_5 y^2_i + \beta_6 y^3_i + \beta_7 y^3_i + \beta_8 y^3_i + \beta_9 y^3_i + \varepsilon(x_i, y_i) \quad (8)$$

Local polynomial:

The conceptual basis for Local Polynomial interpolation is to fit many smaller overlapping polynomials, and then use the center of each polynomial as the prediction for each location in the study area, as opposed to the global polynomial method which fits a polynomial to the entire surface. The resulting surface will be more flexible for local variation compared to a global polynomial (Johnston *et al*, 2001).

Inverse Distance Weighted (IDW):

IDW interpolation is a local interpolation method strictly based on Toblerôs first law of geography (equation 10). Each cell in the matrix is calculated by using the measured values of the neighboring cells. Points closer to the prediction location will have greater influence than more distant points (Johnston *et al*, 2001). Thus, the inverse distance between the unknown

value and the surrounding cells is used as weight. This relationship is explained by the following formula (Eklundh 2001):

$$z(x_p) = \frac{\sum_{i=1}^{n} z(x_i) * \frac{1}{d^k}}{\sum_{i=1}^{n} \frac{1}{d^k}} \qquad (10)$$

Where:

$z(x_p)$ is the interpolated value,

n is the number of points used,

$z(x_i)$ is the value for point *i*,

d is the distance between point *i* and point *p*, and

k is a power determining the dependency of the distance.

Ordinary Kriging:

Ordinary Kriging is a geostatistical interpolation method, based on the semivariogram (equation 11). It assumes the following model (Johnston *et al*, 2001):

$$Z(s) = \varepsilon + \delta(s) \qquad (11)$$

Where:

ε is an unknown constant and,

δ(s) represents random fluctuations.

Ordinary Kriging forms weights from the surrounding measured values to predict values at unmeasured locations, similar to IDW interpolation. The closest measured values usually have the most influence. However, the kriging weights for the surrounding measured points are more sophisticated than those of IDW. IDW uses a simple algorithm based on distance, but in kriging the weights are defined by studying the dataset in a semivariogram (see section 3.6.3 for an explanation of semivariogram analysis) (Johnston *et al*, 2001).

Thiessen polygons:

Thiessen polygons is a simple interpolation method. Polygons divide an area into irregular homogeneous patches around the locations of known values. The polygons define the area

around the point which they are created, and are given the value of the point. The boarder lines distinguishing the polygons are located at the same distance between the two nearest points (Eklundh, 2001).

3 Methods

3.1 Distribution of field investigation sites

The distribution of field investigation sites was made in order to take two main effects into account. Firstly, a representative distribution, i.e. an even distribution of sampling points over the entire area was desired. Secondly, accessibility had to be considered due to the heterogeneous terrain, the sometimes very dense vegetation, and the lack of infrastructure. The latter disabled distribution of points through random selection. A paper topography map in 1:50,000 -scale was available, showing paths and tracks, enabling determination of sampling point accessibility. The number of sampling points was a trade-off between time and magnitude. Since there was a lack of roads in the area most sites had to be reached by foot. An estimation of an average of 3 measurements per day was made. 100 sampling points were manually distributed over 25 km^2, and on-screen digitized in a GIS. This corresponded to approximately 35 working days of field measurements. The coordinates of the sampling points were positioned in the local reference system NAD27, enabling localization during the field campaign. The lack of accessibility, made the availability of sampling points quite heterogeneous, and rather poor in some areas (fig 12).

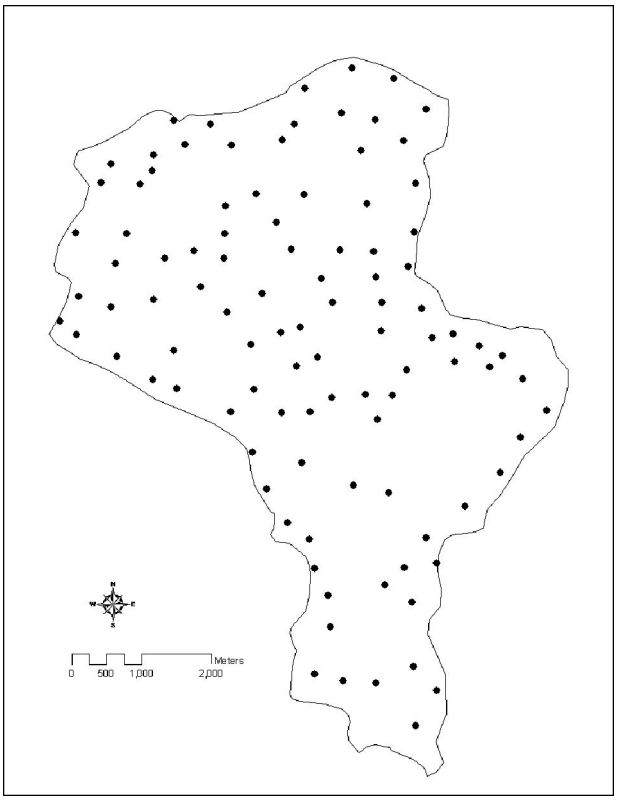

Figure 12: Distribution of sampling points in the study area of Santo Domingo, Central Nicaragua.

The sampling sites were localized with GPS, after which a location as close as possible was chosen. Many locations had to be changed due to obstacles in the terrain which were not possible to overcome (such as rivers, extremely steep slopes and hills, and dense vegetation etcetera). The locations of the sampling sites were recorded in both NAD 27 and WGS 84.

3.2 Saturated hydraulic conductivity

Saturated hydraulic conductivity (K_{sat}) was measured with a Compact Constant Head Permeameter (CCHP), also known as amoozemeter (fig 13). The CCHP enables measurements of K_{sat} in the unsaturated zone. The procedure is known as the constant-head well permeameter technique. It can also be referred to as shallow well pump-in technique, borehole permeameter, or borehole infiltration test (Amoozegar, 2001).

In the constant-head well permeameter technique, the steady state flow rate (Q) of water under a constant pressure (H) (fig 13) under the bottom of a cylindrical hole of radius (r) (fig 14) is measured.

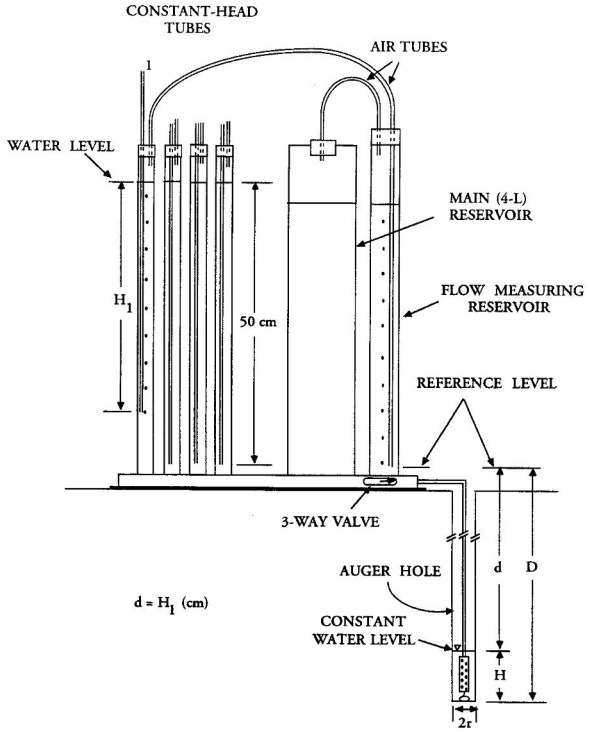

Figure 13: Schematic diagram of the Compact Constant Head Permeameter. From Amoozegar, 2001.

At each site a hole was augured, with a diameter of 6cm. The intention was to make each hole just less than 50 cm deep, in order to create as homogeneous conditions as possible between measurements. Sometimes, however, this was not possible due to a very thin weathering horizon. In these cases the depth could be as shallow as 20cm. After cleaning the bottom of the hole, the depth was measured (D) (fig 13). The water-dissipating unit was then put into the hole, and was switched on. After a while, normally between 20-60 seconds, sometimes longer depending on the physical properties of the soil, a constant water level was reached (H). This water level was then maintained throughout the whole measuring procedure, and is referred to as constant head of water. The distance from the reference level to the surface of this constant water level was measured (d) (fig 13), which was used to set the hydraulic head on the CCHP.

After the constant head of water was established, the infiltration rate was determined. This was done by measuring the change in the height of water with time in the flow-measuring reservoir (fig 13). The change was noted at a certain time interval, which depended upon the rate of change. This was repeated until steady-state flow rate was achieved. When the steady-state flow rate is reached, saturated conditions occur, in the form of a saturated bulb around the bottom of the hole (fig 14).

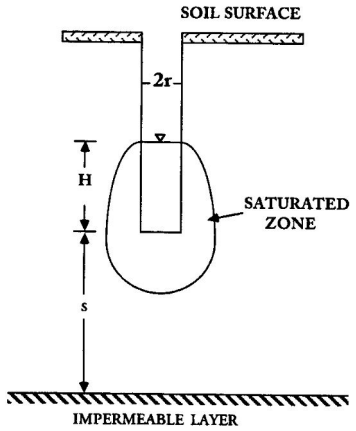

Figure 14: The saturated bulb of water around the bottom of the augured hole, which occurs when steady-state flow rate is reached. From Amoozegar, 2001.

The steady-state flow rate is reached when three consecutive measurements of the flow rate are the same. For an ideal situation, the rate of water flow from an auger hole in the unsaturated zone under a constant head will gradually decrease with time, and approach a final value (fig 15), known as the steady-state flow rate (Q). Depending on the soil properties,

the steady-state flow rate may be achieved in a few minutes to a few hours. In some cases (e.g. in heavy clays) no water flow may occur after the constant head is established in the hole. In other cases, steady-state flow may be reached very quickly, and the water flow is very fast (e.g. soils dominated by sand) (Amoozegar, 2001). Therefore, during the field campaign the measurement interval varied from as low as 1 minute up to 30 minutes, depending on the physical properties of the soil.

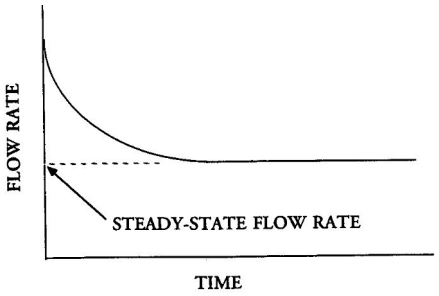

Figure 15: Steady-state flow rate. In field, steady-state flow rate was considered to be reached when three consecutive measurements in a row showed the same value. From Amoozegar, 2001.

K_{sat} was calculated with the Glover Solution (equation 12), using the field data. In the Glover Solution K_{sat} is the only unknown parameter. Hence, there is no need to estimate or use an independent method to obtain a second parameter related to the unsaturated flow around the auger hole. Moreover, the Glover Solution is independent of the soil texture and structure. Thus, there is no need to estimate soil structure and texture to obtain a coefficient, or constant factor for determining K_{sat} (Amoozegar, 2001).

The Glover Solution is given by:

$$Ksat = AQ \qquad (12)$$

Where:

$A = \{\sinh^{-1}(H/r)$ ï $[(r/H)^2 + 1]^{1/2} + r/H\}/(2\pi H^2)$

Q = steady-state of water flow from the permeameter into the auger hole

In the equation above, $\sinh^{-1}$ is the inverse hyperbolic sine function, and r and H are as defined earlier (fig 13) (Amoozegar, 2001).

The Glover Solution only depends on the depth of water in the hole (H), the radius of the hole (r), and one measurement of the steady-state flow rate (Q), which makes it easily evaluated. Since the method has been widely used (e.g. Godsey and Elsenbeer, 2002, Mulqueen and Rodgers, 2004, or Sobieraj 2004), a coefficient for A at different r values has been developed. Hence, in this investigation A could be derived without using the equation mentioned above.

3.3 Slope measurements

A clinometer was used to determine the slope at each study site. Slope was noted in both degrees and percentage. Depending on the roughness of the landscape and the density of the vegetation, as well as other factors influencing visibility, slope was measured on a transect ranging from 10-50m.

3.4 Particle size analysis

At each site a soil sample was taken at the bottom of the auger hole, with a sampling auger. The fraction of fine particles in the soil samples was analyzed. The soil samples were dried, and then grinded in a mortar. Each sample was subsequently weighted after which they were sieved with water through a 75μm sieve. The sieving enabled distinction between sand and silt according to the Unified Soil Classification System. The 75μm sieve was the finest sieve available at the lab in Managua. The remainder of the sample after the sieving procedure was dried, weighed, and subtracted from the weight of origin. The result was called fraction of fine particles, expressed as a percentage of the entire sample. The permeability of clays is known to be highly affected by commingling of non-clay sediments (Neuzil, 1994). The hydraulic conductivity should therefore be higher in samples with a smaller fraction of fine particles.

3.5 Preparation and collection of digital data

Geographical digital data of the study area was available through Alfredo Mendoza at CIGEO and from Instituto Nicaraguence de Estudios Territoriales (INETER). The majority of the data was available in MapInfo format (appendix 1). A number of datasets were created throughout the project (appendix 2). The data provided by CIGEO and INETER was trusted in terms of accuracy.

In this project Arc view 3.3, ArcGIS 8.3, and ArcGIS 9, was used. Therefore conversions between MapInfo and Esri format had to be made. This was made in MapInfo professional 7.0. Moreover, the data was available in two different reference systems, NAD 27 and WGS 84. One of them had to be transformed, since it is only possible to work in one system. Therefore, the data with the reference system NAD 27 was transformed to WGS 84, with arc toolbox in ArcGIS 9.

3.6 GIS and data analyses

The K_{sat} sampling points were digitized as a point layer with WGS84 coordinates in a GIS. In order to identify the sampling points in the different geological features of the area, the layers with geological data were rasterized in ArcGIS 9. 50 meters wide buffer zones were created around the fractures and the quartz veins as a general approximate of their width (see figure 5, for specific locations of all the known fractures and quartz veins of the study area). The geological features were also reclassified, and all cells were given the value 1. This enabled identification of where each sampling point was located in terms of geology. The identification was done through overlay operations with the application ñraster calculatorò in ArcGIS 9. This material was later used to compare different geological units in terms of K_{sat} (see chapter 3.7).

In order to match the sampling points with individual values for height, an overlay operation was made, where a rasterized dataset with sampling point number as attribute was multiplied with a Digital Elevation Model (DEM). The construction of the DEM is explained more in detail below.

3.6.1 Construction of the DEM

The original material when constructing the DEM was received from Alfredo Mendoza, CIGEO, as digitized topographic contour lines with an equidistance of 10 meters. These originated from maps provided by INETER. The interpolation was created with the topogrid module in Arc Info workstation, based on the ANUDEM (Australian National University Digital Elevation Model) program. The output resolution is limited to the equidistance of the input contour data, in this case 10 meters. A DEM with an output grid spacing of 10 meters was therefore created.

The ANUDEM is an iterative finite difference interpolation technique. It is founded on a thin plate spline interpolation method, where a roughness penalty is used to allow the fitted DEM to follow abrupt changes in terrain, such as streams and ridges. It has the computational effectiveness of local interpolation methods such as inverse distance weighted interpolation, without losing the surface continuity of global interpolation methods such as kriging and splines (ESRI, 2004). The ANUDEM is particularly designed for the construction of hydrologically correct DEM:s, with realistic drainage properties from a relatively small number of input data sets (Kienzle, 2004).

The ANUDEM algorithm applies a nested grid strategy where DEM:s are calculated at consecutively finer resolutions, and thereby combining global and local interpolation methods. This is done by starting the iteration at an initial coarse grid and halving the pixel size until the user-specified resolution is attained. Additionally, the ANUDEM eliminates pits and uses stream information to make sure that the resulting DEM is hydrologically accurate. Since most terrains have been shaped geomorphologically by running water, this method is superior to other purely mathematically based models (Kienzle, 2004). A drainage enforcement algorithm removes incorrect depressions and false sinks from the DEM, in order to stipulate the interpolation process to produce a hydrologically correct terrain (Kienzle, 2004).

The topogrid module of ESRIôs ARC INFO was used to perform the interpolation. In the topogrid module there were three user-supplied tolerances for the drainage algorithm to be set. First, the boundaries of the output DEM was set to respond to the boundaries of the input data. Secondly, a tolerance reflecting the accuracy of the input data had to be set. It is recommended to set this boundary to half the contour interval when using contours as input data (ESRI, 2004). This tolerance was set to 5 since a contour interval of 10 meters was used as input data. Thirdly, tolerances for horizontal and vertical standard errors had to be set. The horizontal error represents the amount of error inherent in the process of converting line elevation data into a regularly spaced grid. It is scaled by the program depending on the local slope at each data point and the grid cell size (ESRI, 2004). The vertical error represents the amount of non-systematic, or random, error in the Z-values of the input data. These two tolerances were left with their default values since they have been tested with a wide variety of data sources, and therefore shown to be very robust (Esri, 2004).

3.6.2 Evaluation of the DEM

A commonly known problem associated with DEM: s, interpolated from line topographic data is the occurrence of terracing (Eklundh and Mårtensson, 1995). The terracing originates from the uneven distribution of data points in line topographic data. The data points are very dense along the topographic lines, and scarce perpendicular to the lines, especially in areas of low relief. This may create unnatural terraces in the DEM, and consequently the DEM may not resemble the natural landscape. Therefore the produced DEM was examined for unnatural terracing. This was done by visually studying the DEM. Areas that seemed to be experiencing unnatural terracing, was studied at a close level. A 280 meter transect was drawn perpendicular to the slope, with the ñ3D analystò tool in ArcGIS 9. The transect could then be plotted in a height versus distance ï graph. The area, which looked the most terraced, was further analyzed by zooming in at the region around the brake point. Another transect was drawn, this time 80 meters long, with a brake point at 100 meter distance in the previous transect. In this way the level of terracing could be studied at a very detailed scale.

The most common evaluation of this kind of data is to create contours from the new surface and compare them to the input contour data. These new contours are preferably created at half the original contour interval, whereby the results between contours can be examined. By drawing the original contours and the newly created contours on top of one another identification of interpolation errors can be identified (ESRI, 2004). Contours at a 5 meters interval were generated with surface analyst in ArcGIS 9, and visually compared with the original contours.

The third and last evaluation method carried out was to compare the output DEM with known streams. The river dataset was overlayed on top of the DEM to see whether or not the streams ran through the valleys created in the interpolation.

The GPS used in the field study was not technically advanced enough to take reliable height measurements, and thus it was not possible to collect a training data set in field.

3.6.3 Autocorrelation of K_{sat}

In order to study spatial relationships between values of K_{sat} at different locations, an experimental semivariogram was applied to the Ksat data. The experimental semivariogram enables analysis and quantification of the autocorrelation in continuous data. Basically it tests Toblerôs first law of geography, which states that everything is related, but near things are more related than distant things (Tobler, 1970).

The method is based on semivariance, which is a statistical function of the distance separating two observations for a variable. The semivariance is defined with the following formula:

$$\gamma(h) = \frac{1}{2m}\sum_{i=1}^{m}[z(x_i) - z(x_i + h)]^2 \qquad (13)$$

Where:
$\gamma(h)$ is the semivariance,

m is the total amount of possible comparisons between pairs in the data,

$z(x_i)$ is the value of attribute z in point x_i, and

h is the distance between two points (Eklundh, 2001).

The experimental semivariogram is a plot of semivariance versus distance (fig 16). If autocorrelation exists the semivariance is low for short distances, and the difference between the measured parameter increases with the distance between the pairs.

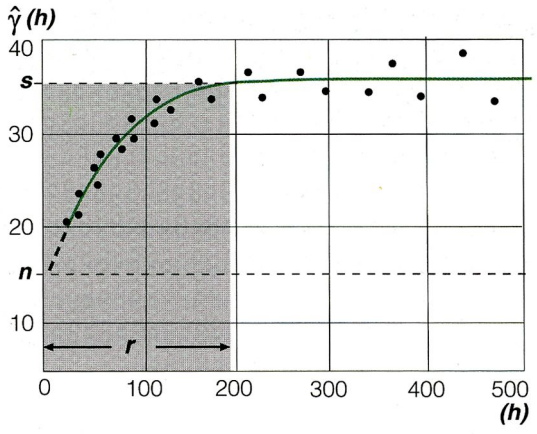

Figure 16: Experimental semivariogram showing semivariance ϒ(h) on the y-axis and distance between pairs (h) on the x-axis. The data values experience a high spatial dependence, since values to the left on the x-axis show low semivariance ϒ(h), and values to the right on the x-axis experience highϒ(h). S=sill, r=range, and n=nugget. From Eklundh, 2001.

Three parameters are used to mathematically model the experimental data: nugget, sill, and range (Zapata and Playán, 2000). The nugget is the distance for a value equal to zero, where the curve crosses the y-axes in the semivariogram (fig 16). A non-zero nugget indicates a systematic measurement error or the existence of spatial variation at a smaller scale than measured. This is a measure of the spatially uncorrelated noise. In other words, this is the variance of measurement errors combined with that from spatial variation at distances much shorter than the sample spacing, which cannot be resolved (Burrough and Mc Donnell, 1998). This variation can be interpreted as a result of the stochastic error present within the data. If a great deal of the variance is made up by nugget, the random variation is so high that interpolation of the data is meaningless (Eklundh, 2001).

Sill is the horizontal value for the lag where the curve levels off in the semivariogram (fig 16). At these values of the lag there is no spatial dependence between the data points because all estimates of variances of differences will be independent of sample separation distance (Burrough and Mc Donnell, 1998).

The curve in figure 16 climbs from a low value of $\Upsilon(h)$ to the sill, arriving at range, which is the corresponding value on the x-axis. This part of the semivariogram describes how inter-site differences are spatially dependent. The closer sites are within the range, the more similar they are likely to be. Values outside of range lack spatial dependence (Burrough and Mc Donnell, 1998). Range can be used to identify the appropriate with of the search window in e.g. an IDW interpolation.

Geostatistical analyst in ArcGIS 9 was used to explore the in field collected data of K_{sat} in an experimental semivariogram. If spatial correlation exists pairs of points that are close together, to the left of the x-axis in the semivariogram should be alike, i.e. low on the y axis. On the other hand, if the pairs of points produce a horizontal straight line, or a box like appearance there may be no spatial correlation in the data (Johnston, 2001).

3.6.4 Interpolation of K_{sat}

Locations with unknown values of K_{sat} were interpolated with Esriôs spatial wizard and geostatistical wizard -tools in ArcGIS 8 and 9. The methods used were: ordinary kriging, global polynomial, local polynomial, thin plate spline, inverse distance weighted, and thiessen

polygons (see section 2.2.1 for descriptions of how the methods work). For the global and the local polynomial interpolations, first order (linear), second order (quadratic), and third order - polynomials (cubic) were tested.

3.6.5 Evaluation of interpolation models

Cross validation was used in order to compare the different interpolation techniques, and to choose the most appropriate method. Cross validation provides with calculated statistics serving as indicator whether the model and/or its associated parameter values are reasonable (Johnston *et al,* 2001). For all points used in the dataset, cross-validation sequentially omits a point, predicts its value using the rest of the data, and then compares the measured and predicted values (Esri, 2004). Hence, no training dataset is required for validation of the interpolation method. Root Mean Square (RMS) error (equation 14) and mean predicted error (equation 15) is given for all the interpolation methods available in Esriôs Geostatistical wizard. For models that provide the most accurate prediction, the mean error should be close to 0, and the RMS error should be as small as possible (Johnston *et al*, 2001). The mean error can be a positive as well a negative number. In this way different types of interpolation methods were compared. The following formulas explain how the mean and RMS -errors are calculated:

Mean predicted error:

$$\frac{\sum_{i=1}^{n} Z(s_i) - z(s_i)}{n} \qquad (14)$$

RMS predicted error:

$$\frac{\sqrt{\sum_{i=1}^{n} Z(s_i)} - z(s_i)}{n} \qquad (15)$$

Where:

$Z(s_i)$ is the predicted value from the cross validation for location s_i,

$z(s_i)$ is the observed value for location s_i, and

n is the number of locations (Johnston *et al*, 2001).

Comparisons between interpolation methods were not exclusively made through cross validation. An additional method was used, to investigate possible differences or similarities between interpolation techniques. The very simple interpolation method known as thiessen polygons were compared with the more complex kriging method in a scatter plot graph. The values of thirty randomly distributed points were used.

3.6.6 Global trends

The K_{sat} sampling points were examined for global trends through trend analysis, with the Trend tool in Geostatistical analyst, ArcGIS 9. With this tool it is possible to project the sampling points in two directions, in a three-dimensional plot of the study area. The points are raised above the study site to the height of the values of the attribute of interest, after which they are projected in two directions onto planes that are perpendicular to the map plane. A polynomial curve is fit to each direction (Johnston, 2001). In this way it is possible to see if there are any global trends in the data.

If a global trend exists it can be removed from the data when interpolating with a geostatistical method, enabling concentration on the random short-range variation, i.e. autocorrelation, only. On the other hand, a global trend itself can be interesting to model with a deterministic method such as a global or local polynomial interpolation method.

3.7 Data and statistical analyses

Data and statistical -analyses were performed to facilitate comparisons between K_{sat} and the other parameters measured and collected in situ. Scatterplots were created in order to compare K_{sat} versus fraction of fine particles, elevation, and slope. In order to study the frequency distribution of K_{sat}, a histogram was created. A histogram helps to visualize how the measured data is distributed, and within what range the highest, as well as the lowest values are found.

The K_{sat} distribution in terms of geological regions and features were analyzed in a Kruskal-Wallis test to see whether they significantly differed from each other or not. Kruskal-Wallis is a non parametric test that examines differences between three or more groups or conditions.

The test provides with a P-value (asymptotic significance), number of degrees of freedom, as well as a value for chi-square.

In order for the difference to be significant the P-value should be less than 0.05. With a $P < 0.05$ the null hypothesis that a set of samples originates from the same population can be disregarded. The Kruskal-Wallis test was chosen since the data showed not to be normally distributed. The more commonly used ANOVA-test assumes that the data is normally distributed, and could therefore not be used on this data. The statistical analyses were performed in Excel and SPSS.

4 Results

4.1 Frequency distribution of K_{sat}

Values of K_{sat} ranged from 0.0028 cm/h (7.8 * 10^{10} m/s) to 10.43 cm/h (2.9 * 10^{-6} m/s) (fig 17). The study area was dominated by low values of K_{sat}, 58% of the samples showed a K_{sat} lower than 0.34 cm/h (9.4 * 10^{-8} m/s), and 68% showed a K_{sat} lower than 1 cm/h (2.78 * 10^{-7} m/s). Only 17% of the samples showed a K_{sat} above 2.67 cm/h (7.42 ó10^{-7}). Around 10 cm/h (2.7 * 10^{-6} m/s) there was a peak of sampling points, representing 5 % of the total samples (see section 4.5.1 fig 29, for geographical distribution). The mean value of K_{sat} was 1.4 cm/h (3.89 * 10^{-7}) with a standard deviation of 2.39 cm/h (6.64 * 10^{-7} m/s) (for reference values, see sectio

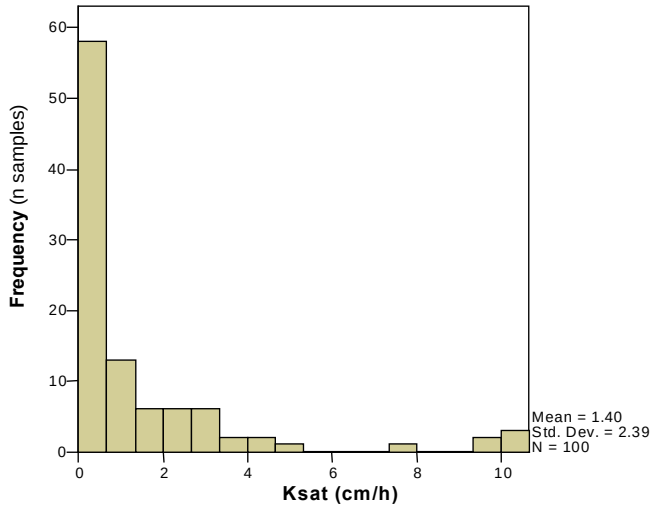

Figure 17: Frequency distribution of $K_{sat.}$ Note that more than 50% of the samples fall under a K_{sat} of 0.33 cm/h.

4.2 DEM

The DEM showed a landscape of fairly high relief, creating a branch like system of valleys, which becomes more visual towards the northern areas, as the relief becomes stronger (fig 18). Visually the DEM corresponded well to the real landscape (fig 19). The digitised stream layer corresponded well with the DEM which suggests that the DEM is hydrologically correct (fig 20).

As the DEM was studied closer, terracing effect seemed to be present (fig 21a). However, when altitude versus horizontal distance was studied, the terracing was not particularly strong. As a transect was drawn over a 60 meters elevation distance, a graph with slight terracing was produced (fig 21b). However, when the area of most terracing was studied closer (break point at around 175 meter), at a 2.5 meters elevation distance, there was no terracing found (fig 22 a and b).

The contour lines at half the contour interval of the original map derived from the DEM, corresponded well with the original contour lines (fig 23). In some parts the contour lines from the DEM was somewhat smother and more generalized.

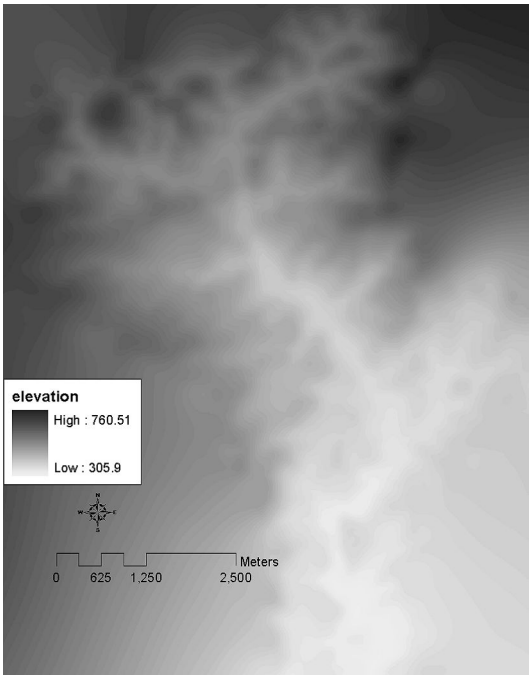

Figure 18: DEM created from contour lines with Hutchinsonôs ANUDEM.

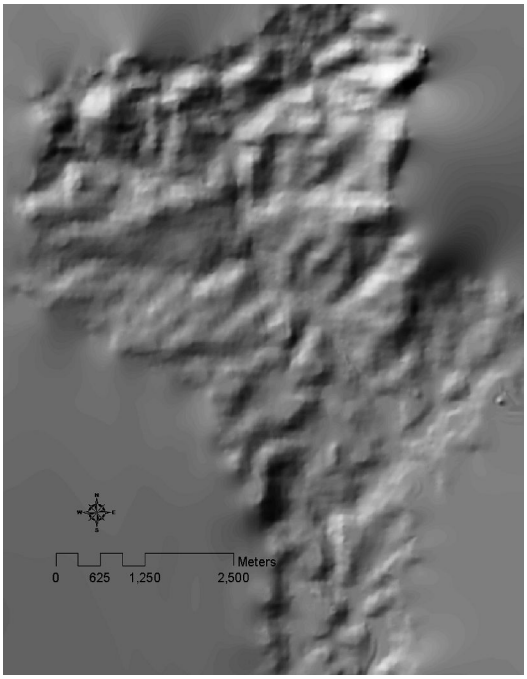

Figure 19: Shaded relief of the DEM.

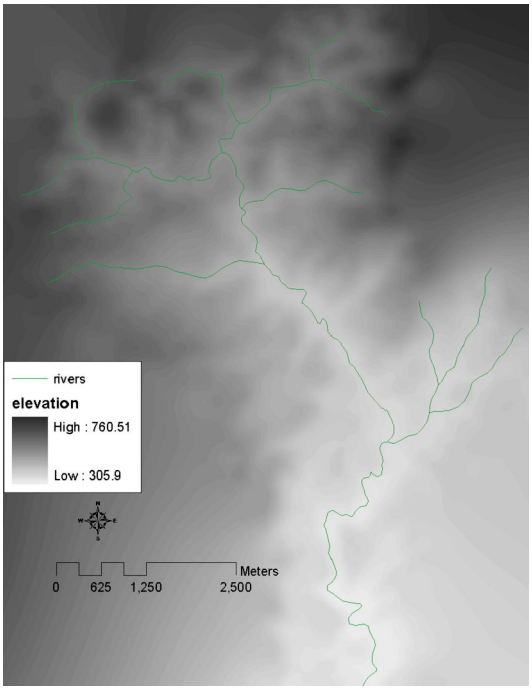

Figure 20: Stream line data set overlaid on top of the DEM. Note that streams follow branch like system created by the interpolation.

a: b:

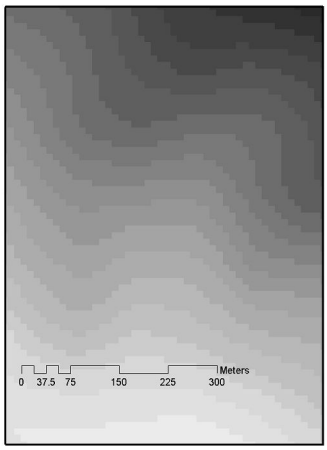

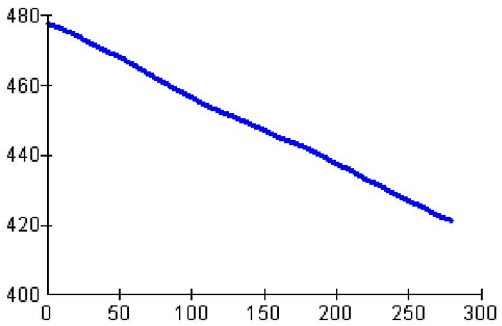

Figure 21: a: Magnification of a 450*700m area. Terracing seems to be present. b: A 300 meter transect was drawn perpendicular to the slope. Slight terracing seems present, for example around 100m on the x-axis.

a: b:

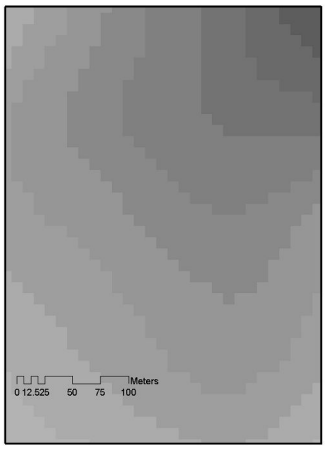

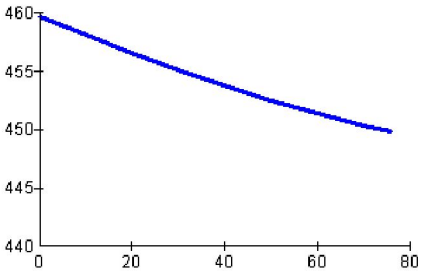

Figure 22: a: The area in figure 15b which seem to experience terracing at 100 meter was zoomed in.
b: and a new transect was drawn, from 60 m to 140m. The slope seems to be rather smooth.

a b

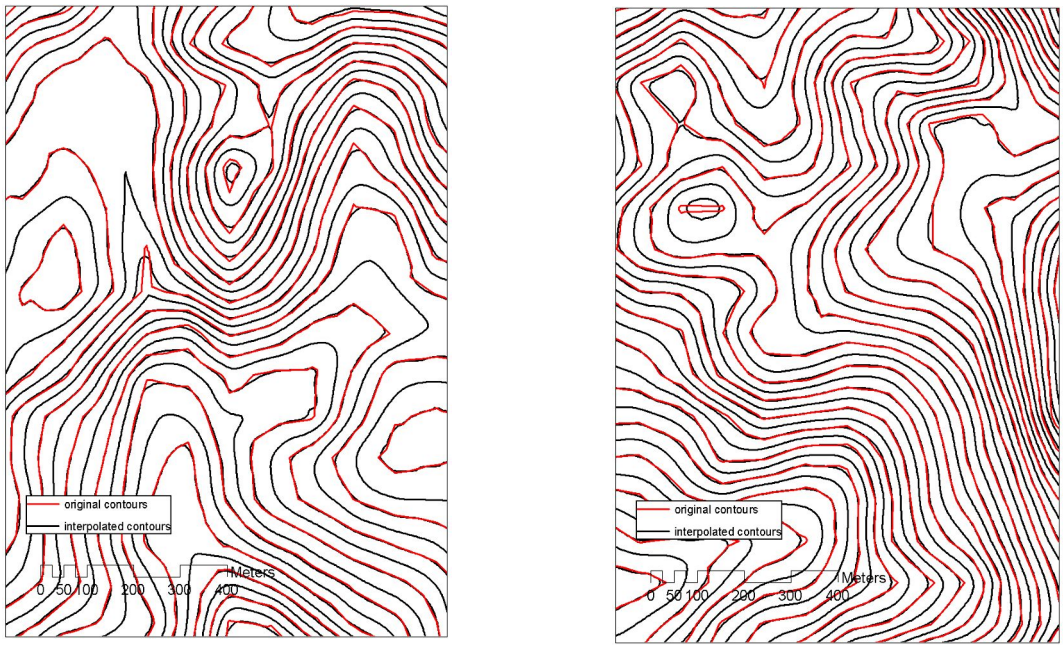

Figure 23 a and b: Contour lines created from the DEM at half the original contour interval (black) matched with the original contour lines (red).

4.3 Correlation between K_{sat} and slope, fraction of fine particles, and elevation

K_{sat} did not show any correlation with slope (fig 24), elevation (fig 25), or fraction of fine particles (fig 26). The K_{sat} -level of around 10 cm/h in figure 24, range in slope between 0 and just above 25 degrees. This means that a level for K_{sat} of 10 cm/h is represented by both the largest and the smallest slope measured, of the entire study area. Figure 25 and 26 show similar patterns suggesting that K_{sat} is not influenced by elevation or the fraction of fine particles. If the higher values in figure 26 are neglected, there is a tendency of a trend where K_{sat} is increasing with fraction of fine particles.

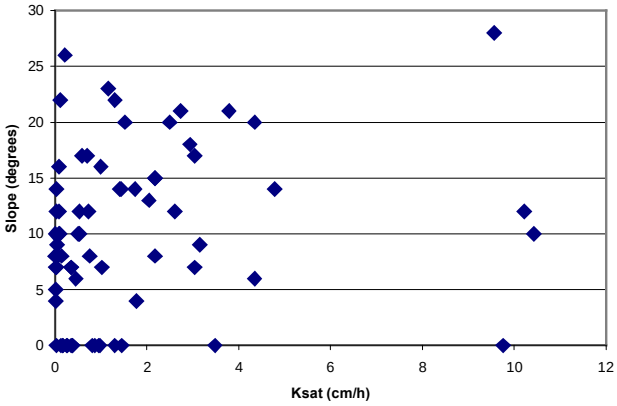

Figure 24: K_{sat} (cm/h) versus slope (°).

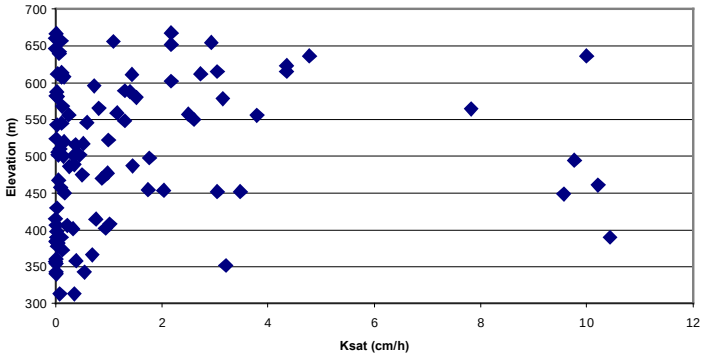

Figure 25: K_{sat} (cm/h) versus elevation (m).

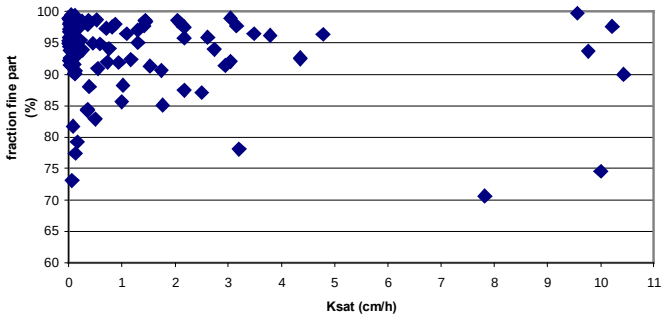

Figure 26: K_{sat} (cm/h) versus fraction of fine particles (%).

4.4 Geological features

Sampling points located in quartz veins generally experienced higher K_{sat} compared to the other features (fig 27 & table 2). Moreover, sampling points located on tuff displayed a much lower K_{sat} than sampling points located in other features. The highest values were found as outliers on bedrock consisting of lavaflow (fig 27). However, the difference between the four groups was not statistically significant. The Kruskal-wallis test of variance gave a P-value, or asymptotic significance, of 0.225, which is well above the threshold-value of 0.05 (table 3). With a P>0.05 the null hypothesis that the samples originates from the same population could not be discarded.

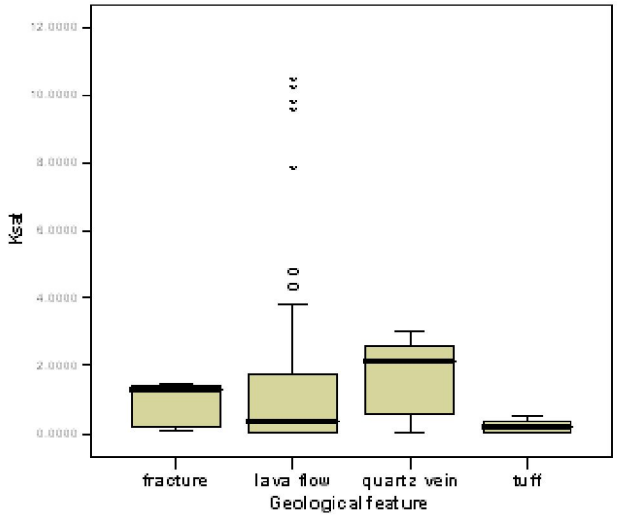

Figure 27: Difference in K_{sat} between the geological features of the area.

Table 2: Difference in K_{sat} between geological features.

Groups	*Count*	*Sum*	*Average*	*Variance*
Fracture	5	4.50156	0.90	0.51
Lavaflow	80	113.6171	1.42	5.96
Vein	6	10.58874	1.76	1.43
Tuff	7	1.40806	0.20	0.05

Table 3: Kruskal wallis test of the difference in K_{sat} between geological features. Note that the P-value, or asymptotic significance, is over 0.05. Df = degrees of freedom.

4.5 Spatial variability of K_{sat}

The semivariogram analysis showed clearly that the spatial dependency between measurements of K_{sat} at different locations is poor. The pairs in the semivariogram formed a box-like scatter, indicating that distance between points was not correlated with K_{sat} (fig 28). It was not possible to find sill, nugget or range in the semivariogram. Hence, there was not much use in interpolating K_{sat}. This was verified by the high RMS errors as the sampling points were interpolated with different methods (table 4). Higher orders of the polynomials, both in the global and the local polynomial method, gave rise to higher RMS and mean errors. Moreover, a sophisticated and mathematically complex interpolation method like kriging did not produce a very distinct result compared to a much simpler interpolation method like thiessen polygons ($R^2 = 0.84$) (fig 29).

Table 4: Interpolation of $K_{sat.}$ Different interpolation methods and statistical evaluation. Lowest error marked in bold text.

Interpolation method	**RMS -error**	**Mean error**
Ordinary kriging	2.383	**0.001811**
Global polynomial 1st power	2.335	0.004756
Global polynomial 2nd power	2.354	-0.008255
Global polynomial 3rd power	2.363	-0.009322
Local polynomial 1st power	**2.327**	-0.05478
Local polynomial 2nd power	2.356	-0.005742
Local polynomial 3rd power	2.365	-0.006853
RBF - thin plate spline	2.358	0.05072
Inverse Distance Weighted	2.388	0.01613

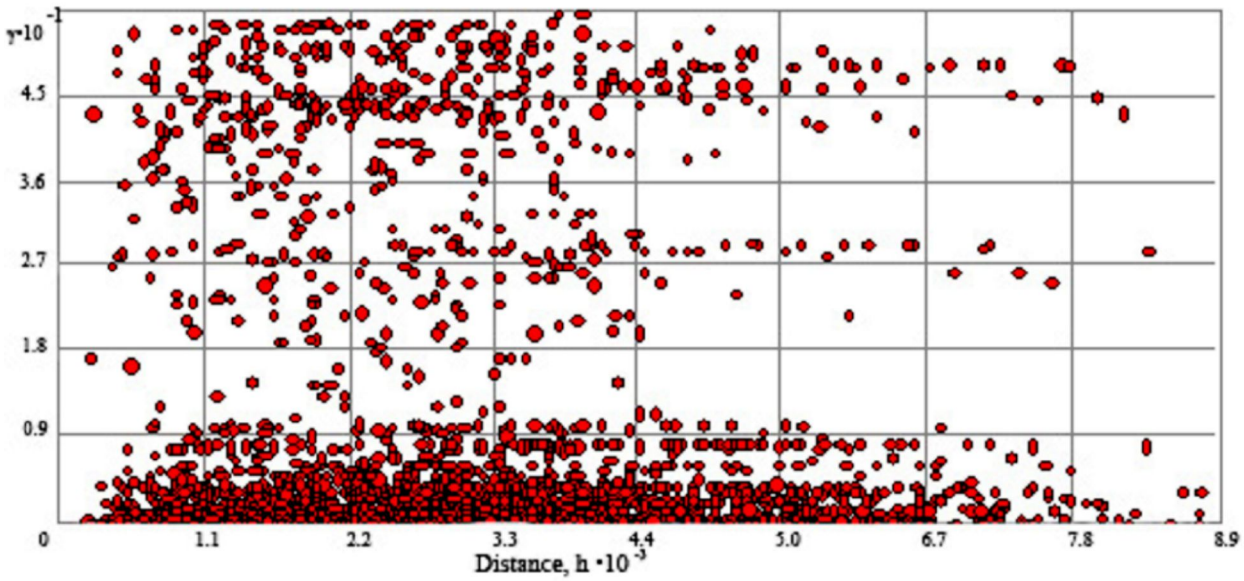

Figure 28: Semivariogram of K_{sat}. The semivariance is displayed on the y-axis, and the distance between pairs on the x-axis.

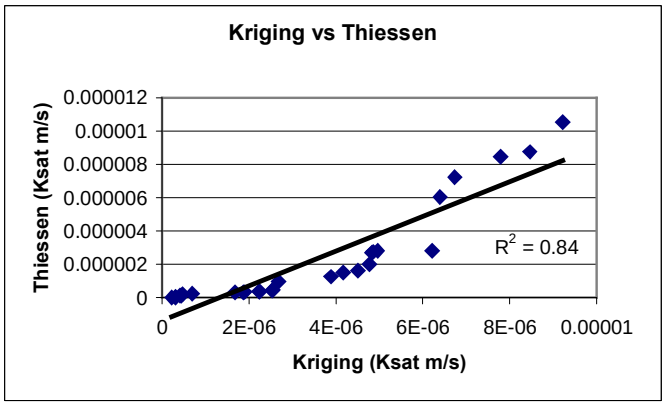

Figure 29: The similarity of K_{sat} interpolation between the results of two distinct interpolation methods is shown. Kriging on the x-axis and Thiessen polygons on the y-axis (R^2=0.84).

4.5.1 Directional trends

The trend analysis showed a global directional trend with low values in the south and higher values towards the northern regions, as indicated by the North-South projected graph (fig 30). Moreover, the East-West projected graph suggested a concentration of higher values of K_{sat} towards the middle of the area, and subsequently lower values towards the eastern and western boundaries. Note however that northern area does not only contain high values, it also contains lower values. Nevertheless, figure 30 shows how the highest values of K_{sat} are geographically distributed.

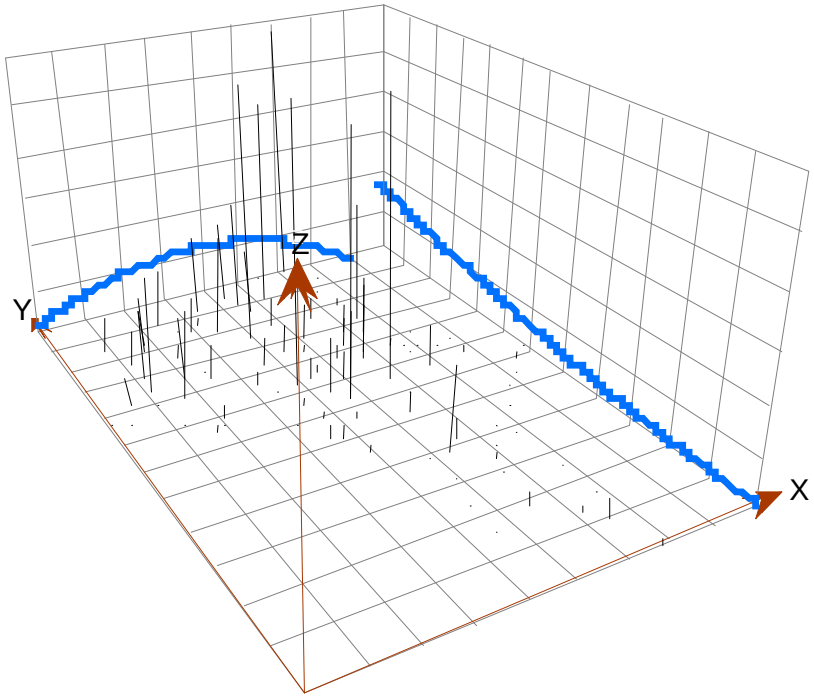

Figure 30: Trend analysis of the K_{sat} sampling results. The y-axis defines the north direction, and the x-axis the east direction, and the z-axis the magnitude of K_{sat}. The blue lines show the directional trends of the data.

5 Discussion

5.1 Frequency distribution of K_{sat}

Throughout the basin the conductivity measurements varied over a range of five orders in magnitude, from 0.0028 cm/h to 10.43 cm/h. The study area was dominated by low values of K_{sat}. However, some sampling points demonstrated very high values of K_{sat} (fig 17). These points were rather small in number, and were found as outliers in areas with bedrock consisting of lava flow (fig 27). Factors explaining these values may be the presence of macropores near the auger holes or external factors affecting the measurements, such as wind which makes the CCHP sway.

Since K_{sat} is a measure of the ability of a soil to conduct water, the generally low values of K_{sat} in the Rio Sucio drainage basin indicate that the infiltration and transport of surface water to ground water is poor. This could develop into a problem in the future as the community grows larger, and the potable water demand increases. Expansion of potable water pumping from the ground water may not be possible. Potable water might have to be dominated by surface water. This may well put the health of the inhabitants of Santo Domingo in risk, since current gold extraction methods cause heavy pollution of the surface water.

On the other hand, it is uncertain to draw conclusions that the overall permeability in the drainage basin is low based on these results. Studies have shown that hydraulic conductivity is highly affected by the scale at which it is measured (Iversen *et al*, Neuzil, 1994, and Sobieraj *et al*, 2004). Measurements showing very low values at laboratory or local scale often correspond to much higher values at the regional scale (Neuzil, 2004). The general low values obtained in this study may well provide with much higher values at a regional flow through the basin.

5.2 DEM

The DEM did not experience much terracing. The contour lines derived from the DEM fit well with the original contours, and the streamlines followed valleys created by the DEM. The DEM was therefore considered valid, and used to identify elevation at each sampling point. The major weakness with the evaluation is that none of the methods give a statistical measure for the accuracy of the DEM. Moreover, the comparison between contour lines may be

somewhat biased. Since the contour lines used to evaluate the model are products from the original contour lines, which in turn are used for comparison. Another possible source of error in the method used is the reliability in the correctness of streamline dataset used for evaluation. In this case INETER was trusted in terms of providing with high quality, updated, and accurate data for the streams in the area.

The best way of evaluating the model would obviously be to have a training data set originating from field measurements. However, equipment for obtaining such data was not available during the field study. Another way would have been to keep some of the contour lines and use them for evaluation. Since the area is rather small however, that would be at the expense of precision in the topography through loss of data. Attainment of accurate values of elevation was the main purpose with the DEM. Thus, data quality was given higher priority than evaluation quality.

Point data is sometimes expressed to be a better source of data than contour lines for interpolation purposes (Eklundh and Mårtensson, 1995). The underlying reason for this opinion is the disequilibrium caused in sampling points when using contour lines, as the density of sampling points will be non-existent between the contour lines. Manual digitising of the contour data into a point data layer would have been an alternative method. However, since the study area has a rather high relief that would have been quite time consuming. Alternatively, an algorithm which thins out the contour lines into a point layer could have been used, another process that is time consuming since it would have been necessary to create the actual algorithm.

The generation of the DEM was not the primary emphasis of the work, a trade off between time and quality was made, where the current method was decided to be the best option, under the present circumstances. Besides, given that the major problem with contour lines being the effect of terracing; it is not definite that a point layer source would have given a better DEM, since the effect of terracing is rather small in this case. This may be attributed to the fact that the relief is fairly high in the study area, which decreases the ratio between the quantity of data along the lines and perpendicular to the lines.

5.3 Correlation between K_{sat} and the parameters; slope, fraction of fine particles, and elevation

Regardless of which of the three factors is studied, one can see that a certain level of K_{sat} is represented by a wide array of values on the x-axis (fig 24, 25, and 26). K_{sat} is therefore distributed in a stochastic manner regarding slope, fraction of fine particles, and elevation.

The fact that K_{sat} did not show any correlation with slope (fig 24), elevation (fig 25), or fraction of fine particles (fig 26), may be attributed to a number of reasons.

In theory particle size and distribution is the major factor influencing hydraulic conductivity (e.g. Grip and Rhode, 2003, Fitzpatrick, 1986, or Marshal and Holmes, 1979). Fraction of particles finer than 75μm was analyzed and tested against K_{sat}. No correlation was found, which is not that surprising since most samples consisted of more than 90% of particles finer than 75 μm.

Since the few very high values of K_{sat} may be a result of macropores hit by chance or errors in the measurement procedure, it is interesting to study fig 26 in particular without the higher values. If the higher values in figure 26 are neglected there is a tendency towards a trend with higher K_{sat} as the fraction of fine particle increases. This is the opposite of what was thought when conducting the study, namely that small particles cause lower conductivity.

Fractures sometimes give rise to higher porosity in soils mainly consisting of clay material, and may therefore also cause high infiltration (Neuzil, 1994). This is supported by the indication of higher K_{sat} in samples with a high fraction of fine particles. However, the trend is very weak, and not statistically supported, and it is therefore not possible to draw any conclusions on based on that result.

A more detailed analysis with a hydrometer showing the dominant particle size may have given a correlation between particle size and K_{sat}. However, the lack of time and resources available for laboratory work made hydrometer analysis impossible in this study.

Since a great deal of the soil samples consisted of fine material, it would have been interesting to study the soil structures of the samples. Soils constituted by clay can have different

infiltration characteristics depending on the amount of aggregation present. The presence of clay mostly indicate a low K_{sat}, but may on the other hand be subjected to cracks and macropores (in comparison to a coarser grained soil), and thus give rise to higher K_{sat}.

The two parameters slope and elevation were tested against K_{sat} with the underlying theory in mind that topography and slope greatly influence the microclimatic properties in the soil, and hence also the physical properties (Casanova *et al*, 2000). Fine textured soils are often found at the bottom of slopes, and have small water intake and large runoff potential (Casanova *et al* 2000). The process of erosion should be greater at higher slopes and thus give rise to a deposition of finer particles at gentle slopes (Casanova *et al* 2000).

The lack of correlation between K_{sat} and these three parameters is probably attributed to a great deal to the investigation method. Particle size has its obvious problem, since hydrometer analysis was not possible to carry through. Concerning slope and topography, the sampling points were distributed in a very heterogeneous environment, with the emphasis of covering the drainage basin. In terms of investigating these parameters it would have been better to make transects in fields as homogeneous as possible, concerning geological, biological, and microclimatological characteristics. In that way the relative height and slope between the sampling points could have been compared and correlated with K_{sat}. Particularly concerning elevation it ought to be crucial whether the values of elevation correlated with K_{sat} are measured on the same hill, or at least on the same side of the drainage basin.

A reason for the difficulty in explaining the factors controlling K_{sat}, may be that the parameters are numerous, and intricately connected. There are studies in the field of hydraulic conductivity showing that factors besides the ones traditionally proved to influence conductivity (see chapter 2.1.3), strongly affect K_{sat}.

Sobieraj *et al* (2004) attribute the differences in K_{sat} to microbial processes, especially in cases with clay rich soils at shallow depth. They also suggest that the classical theory of K_{sat} being mostly influenced by particle size is only true for soils consisting of more than 80% sand.

Correlating K_{sat} with bulk density could be an additional method giving valuable information, since it is a good estimation of the soilôs porosity. Previous studies have used bulk density to

estimate hydraulic conductivity, e.g. Brakensiek et al (1984), Vereecken et al (1989), Jabbro (1992), and Wösten (1999) (Julia *et al*, 2004).

5.4 Geological features

The higher mean value of K_{sat} located in, or in the close vicinity to quartz veins (fig 27), was not proved to be significant by the Kruskal Wallis test (table 3). Figure 27 shows that 3 out of 4 compared groups have a wide range of values represented within the same geological type, tuff being the exception. This result further strengthens the suggestion that K_{sat} is not influenced by the material or condition of the bedrock in the drainage basin. A factor that is most likely affecting the result is the distribution of sampling points. Table 2 shows that the distribution is very heterogeneous, where the majority of the sampling points are located in lavaflow.

Areas around quartz veins seemed to contain coarser material (after looking at, and touching the soil). However, this was not verified by the laboratory analysis. The sampling points located in these areas did not contain an average smaller fraction of particles <75 μm, than sampling points located in other areas. However, a more detailed analysis of dominating particle size may provide a different answer. From a purely theoretical point of view, soils derived from quartz veins ought to consist of coarser material than adjacent soils derived from a parent material mainly consisting of lava flow bedrock, since quartz have a larger scale crystal structure.

A possible explanation may be that the zone underneath the sampling point is affected by quartz vein openings. A large part of the sampling points were located in areas subjected to mining. As a mine is abandoned and covered, the soil conditions get heavily altered, and macropores may be created (Guepert and Gardner, 2001). The presence of macropores may therefore explain the higher values of K_{sat}.

Tuff displayed a generally lower mean value of K_{sat} than the other features (table 2). However, this showed to be statistically insignificant (table 3). Tuff is known to have a high porosity, and thus a high hydraulic conductivity. This is not reflected in the soil characteristics, due to the low values obtained. Since tuff is composed by very fine dust particles and easily eroded, the soil derived from this material ought to be rather fine grained,

possibly explaining the low values obtained. However, the soil layer does not have to be derived from the bedrock underneath. Soil particles weathered from a certain bedrock may be transported and deposited far away from the parent material through geomorphological processes (Strahler and Strahler, 1997). It is therefore rather arbitrary to explain the soil conditions with the type of underlying bedrock.

A different method may provide another result. In this case transects could be made in each area of different geological unit. Each transect ought to consist of the same amount of sampling points in homogenous fields. This would enable a better comparison between K_{sat} of each geological unit.

In terms of quality of geological data used in the study, it may have been valuable to secure that the data was accurate. However, as in the case with the streamline data set there was no reason to doubt the quality and the accuracy of the data obtained by INETER. Geological data is not subjected to fast changes over a short timescale; it was therefore never any reason to doubt that the data would need to be updated.

5.5 Spatial variability of K_{sat}

The semivariogram analysis showed clearly that the spatial dependency between measurements of K_{sat} at different locations is poor (fig 28).

The results showed that the distribution of K_{sat} in the drainage basin is not spatially dependent in the sense that the field data responds to Toblerôs first law of geography.
There was no autocorrelation found between the K_{sat} sampling points in the drainage basin (fig 22). The box-like scatter in the semivariogram made it impossible to determine sill, nugget, or range. Relevant information needed for a geostatistical interpolation method, such as the width of the search window, was therefore impossible to find.

There was no noteworthy difference in terms of interpolation methods used (table 4). The fact that the statistical errors increased with the power of the polynomial used both in the global, and the local ï polynomial method, showed that it was not possible to interpolate these values taking into account any local variation.

The lack of spatial dependency within the data lead to the decision not to present any interpolated map of K_{sat} in the thesis, since this would have been quite misleading information. Since the distribution of K_{sat} appeared to be rather stochastic, a mean value of the entire dataset might as well be used to estimate K_{sat} at an unknown location, rather than using the value from any interpolation model. This was verified by the comparison of the thiessen and the ordinary kriging ï interpolation methods. The two techniques proved to give very similar results, suggesting that a map of thiessen polygons will serve as good as a more sophisticated method in this case.

The reason for the lack of spatial dependence is most likely attributed to the coarse resolution of data points. 100 points were distributed over a 25 km^2 area, subsequently giving an average resolution of 500 meters. Other studies have shown that K_{sat} is dependent on such numerous factors that its distribution almost seems stochastic, at least on a larger scale. Zapáta and Playan (1998) investigated infiltration parameters, hydraulic conductivity being one of them, at a small level basin in Saragossa, Spain. They did not find any spatial dependency between values of hydraulic conductivity, and attributes this to a scale problem. They suggest a spacing of 3m between observations. Sobieraj et al (2004) also suggests that spatial structure in K_{sat} can only be found at a smaller sampling scale, in their case lags smaller than 10 meters.

A finer resolution over a smaller and more homogenous area would perhaps produce a different result, compared to the result in this investigation. However, a resolution finer than 10 meters as suggested above, would be very time consuming, and would have to be confined to a very small area. The study was not conducted or tried over a smaller scale prior to the investigation since this particular method, at the present scale, was commissioned.

During the field investigation, some observations of macropores were made (fig 31). A deeper investigation of macro pores and their relationship with K_{sat} may deliver interesting results. Since the soils are dominated by finer particles, there is reason to suspect macropores as the main factor affecting K_{sat}. Soils with high clay content subjected to decreasing water content govern the conditions for crack formation. The cracks form a network of macropores which will be of great importance for water infiltration (Vogel *et al*, 2005). The soils of the study area clearly fulfill such criteria with alternating rain and dry ï periods, subjecting the soils to decreasing water content, whereby the soil will contract and form crack networks. In fine particle-soils these macro pores would have a very high conductivity compared to adjacent

points. Macro pores could therefore be a possible determinant for the stochastic-like distribution of K_{sat} in the Rio Sucio river basin, since there is a possibility that macro pores were hit by chance during the field campaign.

Figure 31: Soil profile showing cracks in the soil, forming macropores.

5.5.1 Directional trends

The directional trend analysis suggested a global trend towards the northern regions of the catchment area consisting of higher values of K_{sat} (fig 30). The infiltration rate of surface water to the ground water may be higher in these areas. These areas are located just north to the village of Santo Domingo, at a higher level, and are probably crucial for the availability of ground water in the village. In these areas, many of the quartz veins are located (fig 7). This may give rise to higher soil porosity, since the parent material in areas like these is less erodable, creating coarser soil particles in comparison to soils derived from the adjacent bedrock, derived from lava flow. This is also where most of the gold mining activities are located. The extraction of gold and the accompanying pollution of the surface water are also located just north to the village. If this area is where most of the groundwater is originating, as indicated by the trend analysis, the location of the gold processing cooperative may be detrimental to the ground water. However, the quartz veins can only partly explain the higher conductivity. The directional trend shows a peak towards the middle of the sampling area as well. The quartz veins are spread out horizontally, covering a great part of the northern sampling area from the Eastern boundaries to the Western boundaries. The center of the river basin does not contain many quartz veins. This is on the other hand where the largest fractures

are found, possibly explaining the high values. The result of the trend analysis has not been statistically tested. The analysis only roughly shows where the highest values are geographically located. Note that in the northern area where most of the higher samples were found, there were also values of low K_{sat} represented. The semivariance analysis further showed that the samples were not spatially dependent. A higher number of samples, distributed more evenly over the study area may provide a different result. It is therefore very difficult to elaborate on the possible hydrogeological effects of the geographical distribution of these samples of higher K_{sat}.

6 Conclusions

The infiltration characteristics of the unsaturated zone in the drainage basin of Santo Domingo showed to be rather low. However, some areas demonstrated very high infiltration rates, giving a difference of five orders of magnitude between the lowest and the highest values. Most of the locations with higher infiltration were located in the northern part of the study area, resulting in a global directional trend from south to north. The sampling points of K_{sat} did not show any spatial dependence, which unjustified the production of an interpolated K_{sat} map over the drainage basin. K_{sat} did not show any correlation between fraction of fine particles, elevation, or slope. Moreover, K_{sat} did not prove any significant difference in magnitude depending on underlying bedrock type, the presence of fractures/faults or quartz veins.

The lack of correlation between K_{sat} and the investigated factors makes it hard to determine what factors control K_{sat} in the drainage basin with the available data. The literature confirms the complexity of determining factors controlling K_{sat} in the unsaturated zone. In this study many factors have been examined, and yet there are more to be studied. A focus on one factor with a finer sampling resolution would be advisable for future studies in the area.

Since the soils are constituted by clayey material there is reason to suspect that macropores determine the stochastic distribution of higher values of K_{sat}. An investigation of the relationship between macropores and the distribution of K_{sat} is therefore advised for future studies of the drainage basin.

The DEM did not experience much terracing even though a topographic line data layer was used as input data. This was however only confirmed by visual evaluation. The absence of terracing may be attributed to the high relief of the area which smoothes out the disequilibrium between sampling points along the isolines versus perpendicular to the lines.

If there still would be an interest to investigate what factors do control the infiltration characteristics in the unsaturated zone of the drainage basin, a more detailed study of each factor is needed.

The relationship between soil particle size and K_{sat} would be very interesting to know, but requires hydrometer analysis due to the high content of fine particles. Hydrometer analysis is rather time consuming. If on the other hand a clear relationship between soil particle size and K_{sat} would be found, the chances of understanding the infiltration conditions of the area would increase significantly. Collecting a large number of soil samples over the entire study area is much faster and easier done, than increasing the resolution of permeameter sampling.

Considering the relationship between geological conditions and K_{sat} this is probably best done by conducting an equal number of K_{sat} measurements in transects over each studied geological unit. The same procedure would be advised for the relationship of elevation and slope. Regarding K_{sat} autocorrelation, this needs to be performed at a much finer scale in order to find any spatial dependence.

7 References

Amoozegar A 2001 *Compact Constant Head Permeameter, user´s manual* Ksat Incorporated North Carolina.

Aronsson M and Wallner C 2002 *Inventory of springs and hydrochemical investigations of groundwater in the drainage basin of Sucio river, Nicaragua* Master of Science thesis ISRN LUTVG/TVTG--5078ð SE University of Lund.

Burrough P A and Mc Donnell R A 1998 *Principles of geographical information systems* Oxford university press, Oxford.

Casanova M, Messing M, Joel A 2000 *Influence of slope gradient on hydraulic conductivity measured by tension filtrometer* Hydrological processes **14**:155-164.

CIA 2006 *The World Fact Book* Internet source: https://www.cia.gov/cia/publications/factbook/index.html.

Darce M R 1989 *Mineralogical alteration patterns, chemical mobility and origin of the La Libertad gold deposit, Nicaragua* Doctoral thesis no 278 Department of Geology, University of Stockholm.

Eklundh L (red) 2001 *Geografisk informationsbehandling Metoder och tillämpningar* CentralTryckeriet, Borås.

Eklundh L and Mårtensson U 1995 *Rapid generation of Digital Elevation Models from topographic maps* Geographical Information Systems **3**:329-340.

Ferrer M, Monreal E T, Corral Jiménez A S, Meléndez E G *Constructing a saturated hydraulic conductivity map of Spain using pedotransfer functions and spatial prediction* Geoderma **123**:257-277.

Fitzpatrick E A 1986 *An introduction to soil science* Longman Scientific & Technical Essex.

Godsey S and Elsenbeer H 2002 *The soil hydrologic response to forest regrowth: a case study from southwestern Amazonia* Hydrological processes **16**:1519-1522.

Grip H and Rhode A 2003 *Vattnets väg från regn till bäck* Hallgren och Fallgren Förlag AB Uppsala.

Grunander K and Nordenberg E 2004 *Investigations of Groundwater-Surface water interaction in the Drainage Basin of River Sucio, Nicaragua* Master of Science thesis ISRN LUTVDG/TVTGð 5090ð SE University of Lund.

Guepert M D and Gardner T W 2001 *Macropore flow on a reclaimed surface mine: infiltration and hillslope hydrology* Geomorphology **39**:151-169.

INETER 1973 *Estudio Edafológico de la Cuenca del Río Escondido* Instituto Nicaragüense de Estudios Territoriales- Ministerio de Agricultura y Ganadería Departamento de Suelos y Taxonomía / Catastro, Nicaragua.

Iversen B V, Moldrup P and Loll P *Runoff modelling at two field slopes: use of in situ measurements of air permeability to characterize spatial variability of saturated hydraulic conductivity* Hydrological processes **5**:1009-1026.

FM5-410 1993 *Military soils engineering* Internet source: http://www.itc.nl/~rossiter/Docs/FM5-410/FM5-410_Ch4.pdf

Johnston K, Ver Hoef J M, Krivoruchko K, and Lucas N 2001 *Using ArcGIS Geostatistical Anslyst* ESRI, Redland.

Mendoza J A 2002 *Geophysical and Hydrogeological Investigations in the Rio Sucio Watershed, Nicaragua* Licentiate thesis ISRN LUTVDG/TVTGð 10111-SE University of Lund.

Marshal T J and Holmes J W 1979 *Soil physics* Cambridge University Press Cambridge.

Mcbirney A R and Williams H 1965 *Volcanic history of Nicaragua* Geological Sciences **55**:1-65.

Merrill T 1994 (ed) *Nicaragua: a country study* library of Congress, Federal research division Washington DC. http://rs6.loc.gov/frd/cs/nitoc.html.

NOAA 2004 *NOAA Satellite and Information service Mitch: the deadliest Atlantic hurricane since 1780* Internet source: http://lwf.ncdc.noaa.gov/oa/reports/mitch/mitch.html.

Ndiaye B, Esteves M, Vandervaere J P, Lapetite J M, and Vauclin M 2005 *Effect of rainfall and tillage direction on the evolution of surface crusts, soil hydraulic properties and run off generation for a sandy loam soil* Journal of hydrology **307**:294-311.

Perry Castañeda (1997) *Nicaragua Shaded relief* University of Texas at Austin Perry ï Castañeda Library Map Collection Internet source: http://www.lib.utexas.edu/maps/nicaragua.html.

Ramos M C, Nacci S, and Pla I 2003 *Effect of raindrop impact and its relationship with aggregate stability to different disaggregation forces* Catena **53**:365-376.

Schwerdtfeger W 1976 *World survey of climatology. Vol. 12, Climates of Central and South America* Elsevier Amsterdam.

Sobieraj J A, Elsenbeer H, Cameron G 2004 *Scale dependency in spatial pattern of saturated hydraulic conductivity* Catena **55**: 49-77.

Sobieraj J A, Elsenbeer H, Coelho R M, Newton B 2001 *Spatial variability of soil hydraulic conductivity along a tropical rainforest catena* Geoderma **108**:79-90.

Strahler A and Strahler A 1997, *Physical Geography: science and systems of the human environment* Wiley cop. New York.

Tobler W R 1970 *A computer movie simulating urban growth in the Detroit region* Economic geography **46**:234-240.

Vogel H J, Hoffmann H, Leopold A, Roth K 2005 *Studies of crack dynamics in clay soil II. A physically based model for crack formation* Geoderma **125**:213-223.

Zapata N and Playán E 2000 *Elevation and infiltration in a level basin. I. Characterizing variability* Irrigation Science **19**:155-164.

Veseth R 1986, *Erosion reduces water storage and yield potential Chapter 1 Erosion impacts PNW Conservation tillage handbook* WSU Press Washington Pullman.

Weinberg R F, 1992 *Neotectonic development of western Nicaragua* American Geophysical Union Washington DC.

APPENDIX 1: Digital data available for GIS-analysis.

Name	Data type	Format	Projection	Reference system	Origin	Description
bascid1	polygon	MIF	UTM	WGS 84 Zone 16	Mendoza/INETER	Geology - plugs
mata1	polygon	MIF	UTM	WGS 84 Zone 16	Mendoza/INETER	Geology - tuff
fracture	line	MIF	UTM	WGS 84 Zone 16	MendozaINETER	Geology ï fractures/faults
vein	line	MIF	UTM	WGS 84 Zone 16	Mendoza/INETER	Geology - quartz veins
acuencasucioarriba_region	polygon	SHP	UTM	NAD 27 Zone 16	Mendoza/INETER	Boarder line of study area
Topo10	line	MIF	UTM	WGS 84 Zone 16	Mendoza/INETER	Topography lines
Rios	line	MIF	UTM	NAD 27 Zone 16	Mendoza/INETER	Rivers

APPENDIX 2: GIS-data created during the project.

Name	Data type	Format	Projection	Reference system	Producer	Description
samplepoints	point	MIF	UTM	NAD 27 Zone 16	Mendoza /Eckeskog	Proposed investigation sites
allaksat	point	coverage	UTM	WGS 84 Zone 16	Eckeskog	Final investigation sites with number ID and Ksat value as measured in field
lavacomplete	raster	coverage	UTM	WGS 84 Zone 16	Eckeskog	Geology - lavaflow
veinrect	raster	coverage	UTM	WGS 84 Zone 16	Eckeskog	Geology ï quartz veins
plugrect	raster	coverage	UTM	WGS 84 Zone 16	Eckeskog	Geology ï plugs
fractrect1	raster	coverage	UTM	WGS 84 Zone 16	Eckeskog	Geology ï fractures/faults
tuffrect	raster	coverage	UTM	WGS 84 Zone 16	Eckeskog	Geology ï tuff
buffer_of_vein	polygon	coverage	UTM	WGS 84 Zone 16	Eckeskog	50 m buffer of quartz veins
Buffer_of_fracture	polygon	coverage	UTM	WGS 84 Zone 16	Eckeskog	50 m buffer of fractures/faults
allaksatgrid	raster	coverage	UTM	WGS 84 Zone 16	Eckeskog	Ksat value of field investigation sites
pointnumber	raster	coverage	UTM	WGS 84 Zone 16	Eckeskog	Number of investigation site
slope1	point	coverage	UTM	WGS 84 Zone 16	Eckeskog	Slope angle in sampling points (%)
topodem3	raster	coverage	UTM	WGS 84 Zone 16	Eckeskog	DEM - ANUDEM
hillshade3	raster	coverage	UTM	WGS 84 Zone 16	Eckeskog	DEM ï hillshade of topodem3
pointelev	raster	coverage	UTM	WGS 84 Zone 16	Eckeskog	Elevation in each sample point. From DEM.
Inverse Distance Weighting	raster	coverage	UTM	WGS 84 Zone 16	Eckeskog	Interpolation of Ksat
Local Polynomial Interpolation	raster	coverage	UTM	WGS 84 Zone 16	Eckeskog	Interpolation of Ksat
Ordinary Kriging	raster	coverage	UTM	WGS 84 Zone 16	Eckeskog	Interpolation of Ksat
Radial Basis Functions	raster	coverage	UTM	WGS 84 Zone 16	Eckeskog	Interpolation of Ksat
Thiessen	polygon	shp	UTM	WGS 84 Zone 16	Eckeskog	Interpolation of Ksat

Lunds Universitets Naturgeografiska institution. Seminarieuppsatser. Uppsatserna finns tillgängliga på Naturgeografiska institutionens bibliotek, Sölvegatan 12, 223 62 LUND. Serien startade 1985.

The reports are available at the Geo-Library, Department of Physical Geography, University of Lund, Sölvegatan 12, S-223 62 Lund, Sweden.
Report series started 1985.

79. Ullman, M., (2001): El Niño Southern Oscillation och dess atmosfäriska fjärrpåverkan.
80. Andersson, A., (2001): The wind climate of northwestern Europe in SWECLIM regional climate scenarios.
81. Lalloo, D., (2001): Geografiska informationssystem för studier av polyaromatiska kolväten (PAH) i Undersökning av djupvariation i BO01-området, Västra hamnen, Malmö, samt utveckling av en matematisk formel för beräkning av PAH-koncentrationer från ett kontinuerligt utsläpp.
82. Almqvist, J., Fergéus, J., (2001): GIS-implementation in Sri Lanka.
    Part 1: GIS-applications in Hambantota district Sri Lanka : a case study.
    Part 2: GIS in socio-economic planning : a case study.
83. Berntsson, A., (2001): Modellering av reflektans från ett sockerbetsbestånd med hjälp av en strålningsmodell.
84. Umegård, J., (2001): Arctic aerosol and long-range transport.
85. Rosenberg, R., (2002): Tetratermmodellering och regressionsanalyser mellan topografi, tetraterm och tillväxt hos sitkagran och lärk i en studie i norra Island.
86. Håkansson, J., Kjörling, A., (2002): Uppskattning av mängden kol i trädform i en metodstudie.
87. Arvidsson, H., (2002): Coastal parallel sediment transport on the SE Australian inner shelf i A study of barrier morphodynamics.
88. Bemark, M., (2002): Köphultssjöns tillstånd och omgivningens påverkan.
89. Dahlberg, I., (2002): Rödlistade kärlväxter i Göteborgs innerstad i temporal och rumslig analys av rödlistade kärlväxter i Göteborgs artdataarkiv, ADA.
90. Poussart, J-N., (2002): Verification of Soil Carbon Sequestration - Uncertainties of Assessment Methods.
91. Jakubaschk, C., (2002): Acacia senegal, Soil Organic Carbon and Nitrogen Contents: A Study in North Kordofan, Sudan.
92. Lindqvist, S., (2002): Skattning av kväve i gran med hjälp av fjärranalys.
93. Göthe, A., (2002): Översvämningskartering av Vombs ängar.
94. Lööv, A., (2002): Igenväxning av Köphultasjö i bakomliggande orsaker och processer.
95. Axelsson, H., (2003): Sårbarhetskartering av bekämpningsmedels läckage till grundvattnet i Tillämpat på vattenskyddsområdet Ignaberga-Hässleholm.
96. Hedberg, M., Jönsson, L., (2003): Geografiska Informationssystem på Internet i En webbaserad GIS-applikation med kalknings- och försurningsinformation för Kronobergs län.
97. Svensson, J., (2003): Wind Throw Damages on Forests i Frequency and Associated Pressure Patterns 1961-1990 and in a Future Climate Scenario.
98. Stroh, E., (2003): Analys av fiskrättsförhållandena i Stockholms skärgård i relation till känsliga områden samt fysisk störning.
99. Bäckstrand, K., (2004): The dynamics of non-methane hydrocarbons and other trace gas fluxes on a subarctic mire in northern Sweden.

100. Hahn, K., (2004): Termohalin cirkulation i Nordatlanten.
101. Lina Möllerström (2004): Modelling soil temperature & soil water availability in semi-arid Sudan: validation and testing.
102. Setterby, Y., (2004): Igenväxande hagmarkers förekomst och tillstånd i Västra Götaland.
103. Edlundh, L., (2004): Utveckling av en metodik för att med hjälp av lagerföljdsdata och geografiska informationssystem (GIS) modellera och rekonstruera våtmarker i Skåne.
104. Schubert, P., (2004): Cultivation potential in Hambantota district, Sri Lanka
105. Brage, T., (2004): Kvalitetskontroll av servicedatabasen Sisyla
106. Sjöström., M., (2004): Investigating Vegetation Changes in the African Sahel 1982-2002: A Comparative Analysis Using Landsat, MODIS and AVHRR Remote Sensing Data
107. Danilovic, A., Stenqvist, M., (2004): Naturlig föryngring av skog
108. Materia, S., (2004): Forests acting as a carbon source: analysis of two possible causes for Norunda forest site
109. Hinderson, T., (2004): Analysing environmental change in semi-arid areas in Kordofan, Sudan
110. Andersson, J., (2004): Skånska småvatten nu och då - jämförelse mellan 1940, 1980 och 2000-talet
111. Tränk, L., (2005): Kadmium i skånska vattendrag ï en metodstudie i föroreningsmodellering.
112. Nilsson, E., Svensson, A.-K., (2005): Agro-Ecological Assessment of Phonxay District, Luang Phrabang Province, Lao PDR. A Minor Field Study.
113. Svensson, S., (2005): Snowcover dynamics and plant phenology extraction using digital camera images and its relation to CO2 fluxes at Stordalen mire, Northern Sweden.
114. Barth, P. von., (2005): Småvatten då och nu. En förändringsstudie av småvatten och deras kväveretentionsförmåga.
115. Areskoug, M., (2005): Planering av dagsutflykter på Island med nätverkanalys
116. Lund, M., (2005): Winter dynamics of the greenhouse gas exchange in a natural bog.
117. Persson, E., (2005): Effect of leaf optical properties on remote sensing of leaf area index in deciduous forest.
118. Mjöfors, K., (2005): How does elevated atmospheric CO2 concentration affect vegetation productivity?
119. Tollebäck, E.,(2005): Modellering av kväveavskiljningen under fyra år i en anlagd våtmark på Lilla Böslid, Halland
120. Isacsson, C., (2005): Empiriska samband mellan fältdata och satellitdata ï för olika bokskogområden i södra Sverige.
121. Bergström, D., Malmros, C., (2005): Finding potential sites for small-scale Hydro Power in Uganda: a step to assist the rural electrification by the use of GIS
122. Magnusson, A., (2005): Kartering av skogsskador hos bok och ek i södra Sverige med hjälp av satellitdata.
123. Levallius, J., (2005): Green roofs on municipal buildings in Lund ï Modeling potential environmenta benefits.
124. Florén, K., Olsson, M., (2006): Glacifluviala avlagrings- och erosionsformer I sydöstra Skåne ï en sedimentologisk och geomorfologisk undersökning.
125. Liljewalch-Fogelmark, K., (2006): Tågbuller i Skåne ï befolkningens exponering.
126. Irminger Street, T., (2006): The effects of landscape configuration on species

richness and diversity in semi-natural grasslands on Öland ï a preliminary study.

127. Karlberg, H., (2006): Vegetationsinventering med rumsligt högupplösande satellitdata ï en studie av QuickBirddata för kartläggning av gräsmark och konnektivitet i landskapet.

128 Malmgren, A., (2006): Stormskador. En fjärranalytisk studie av stormen Gudruns skogsskador och dess orsaker.

129 Olofsson, J., (2006): Effects of human land-use on the global carbon cycle during the last 6000 years.

130 Johansson , T., (2006): Uppskattning av nettoprimärproduktionen (NPP) i stormfällen efter stormen Gudrun med hjälp av satellitdata.